

Multi-model assessment of the deglacial climatic evolution at high southern latitudes

Takashi Obase^{1,2}, Laurie Menviel³, Ayako Abe-Ouchi¹, Tristan Vadsaria^{1,4*}, Ruza Ivanovic⁵, Brooke Snoll⁵, Sam Sherriff-Tadano⁵, Paul J. Valdes⁶, Lauren Gregoire⁵, Marie-Luise Kapsch⁷, Uwe Mikolajewicz⁷, Nathaëlle Bouttes⁸, Didier Roche⁸, Fanny Lhardy⁸, Chengfei He⁹, Bette Otto-Bliesner¹⁰, Zhengyu Liu¹¹, Wing-Le Chan¹

¹Atmosphere and Ocean Research Institute, The University of Tokyo, Kashiwa, Japan

²Japan Agency for Marine-Earth Science and Technology, Yokohama, Japan

³Climate Change Research Center, The Australian Centre for Excellence in Antarctic Science, the University of New South Wales, Sydney, Australia,

⁴UiT The Arctic University of Norway, Tromsø, Norway

⁵School of Earth & Environment, University of Leeds, Woodhouse Lane, Leeds, UK

⁶School of Geographical Sciences, University of Bristol, University Road, Bristol, UK

⁷Max Planck Institute for Meteorology, Hamburg, Germany

⁸Laboratoire des Sciences du Climat et de l'Environnement/Institut Pierre-Simon Laplace, UMR CEA-CNRS-UVSQ, Université Paris-Saclay, Gif-sur-Yvette, France

⁹Woods Hole Oceanographic Institution, Woods Hole, MA, USA

¹⁰Climate and Global Dynamics Laboratory, National Center for Atmospheric Research, Boulder, USA

¹¹Atmospheric Science Program, Department of Geography, Ohio State University, Columbus, USA

**Now at Biogéosciences, UMR 6282 CNRS, Université Bourgogne Europe, 6 boulevard Gabriel, 21000 Dijon, France*

Correspondence to: Takashi Obase (tobase@jamstec.go.jp)

Abstract. The quaternary climate is characterised by glacial-interglacial cycles, with the most recent transition from the last glacial maximum to the present interglacial (the last deglaciation) occurring between ~ 21 and 9 ka. While the deglacial warming at high southern latitudes is mostly in phase with atmospheric CO₂ concentrations, some proxy records have suggested that the onset of the warming occurred before the CO₂ increase. In addition, high southern latitudes exhibit a cooling event in the middle of the deglaciation (15 - 13 ka) known as the “Antarctic Cold Reversal” (ACR). In this study, we analyse transient simulations of the last deglaciation performed by six different climate models as part of the 4th phase of the Paleoclimate Modelling Intercomparison Project (PMIP4) to understand the processes driving high southern latitude surface temperature changes. As the protocol of the last deglaciation sets the choice of freshwater forcing as flexible, the freshwater forcing is different in each model, thus hindering the multi-model comparison. While proxy records from West Antarctica and the Pacific sector

書式を変更: フォント: (日) + 本文のフォント - 日本語 (MS 明朝), (言語 1) 日本語

of the Southern Ocean suggest the presence of an early warming before 18 ka, only half the models show a significant warming [at this time](#) (~1°C or ~10% of the total deglacial warming). All models simulate a major warming during Heinrich stadial 1 (HS1, 18 - 15 ka) concurrent with the CO₂ increase and with an AMOC weakening in some models. However, the simulated HS1 warming over Antarctica is smaller than the one suggested from ice core data. During the ACR, simulations with an abrupt AMOC increase exhibit a high southern latitude cooling of 1 to 2°C, in relative agreement with proxy records, while simulations with rapid North Atlantic meltwater input exhibit a warming. Using simple models to extract the relative AMOC contribution, we find that all climate models simulate a high southern latitude cooling in response to an AMOC increase with a response timescale of several hundred years, suggesting the choice of the North Atlantic meltwater forcing substantially affects high southern latitudes temperature changes. Thus, further work needs to be carried out to reconcile the deglacial AMOC evolution with the Northern hemisphere ice sheet disintegration and associated meltwater input. Finally, all simulations exhibit only minimal changes in Southern Hemisphere westerlies and Southern Ocean meridional circulation during the last deglaciation. Improved understanding of the processes impacting southern high atmospheric and oceanic circulation changes accounting for deglacial atmospheric CO₂ increase are needed.

1. Introduction

The recent Quaternary climate is characterised by glacial-interglacial cycles of about 100,000-year periodicity (Lisiecki and Raymo, 2005; Jouzel et al., 2007). These glacial-interglacial cycles are driven by insolation changes as external forcing and by feedbacks, including changes in atmospheric greenhouse gas (GHG) concentrations and continental ice sheets (Abe-Ouchi et al., 2013). During the Last Glacial Maximum (LGM, ~21 ka; ka indicates 1000 years before present), the continental ice sheets covered a significant area of the high northern latitudes (Tarasov et al., 2012; Peltier et al., 2015), thus leading to a sea level fall of ~130 meters compared to pre-industrial (Lambeck et al., 2014). The atmospheric CO₂ concentration was also ~100 ppm lower than pre-industrial (Petit et al., 1999; Bereiter et al., 2015). These climatic boundary conditions contributed to a colder climate during the LGM, with global mean surface air temperature anomalies estimated to be 4 to 7 °C lower than present-day (Annan et al., 2022; Liu et al., 2023). As the last deglaciation (transition from the LGM to the early Holocene,

[~11 ka](#)) represents one of the largest, most recent and well-documented natural warming of the last million years, an understanding of the processes and feedbacks during this time period can offer insight into our own modern changing world. Here, we focus on the high southern latitudes, where deglacial warming began before their Northern Hemisphere (NH) counterparts (Shakun et al., 2012), and which have been suggested to play a major role in driving the increase in atmospheric CO₂ concentration. Although the timing of the onset of the deglacial warming at high southern latitudes is poorly constrained, a compilation of Antarctic ice core records from East Antarctica suggests that the deglacial Antarctic warming started at ~ 18 ka, in phase with the rise in atmospheric CO₂ concentration (Parrenin et al., 2013). On the other hand, a record from the West Antarctic Ice Sheet Divide ice core (WDC) suggests that the warming started at ~ 20 ka (Shakun et al., 2012; WAIS project members, 2013). Moreover, an early onset of the deglacial warming (~21 ka) at high and mid-southern latitudes has also been suggested based on SST and sea ice records from the Pacific sector of the Southern Ocean (Moy et al., 2019; Sikes et al., 2019; Moros et al., 2021; Crosta et al., 2022; Sadatzki et al., 2023).

Millennial-scale climate events are superimposed on the deglacial warming. At the beginning of the deglaciation, during Heinrich stadial 1 (HS1, ~18 to 14.7 ka, following Ivanovic et al., 2016), Greenland and the North Atlantic region remained cold (Buizert et al., 2014; Martrat et al., 2007), while significant warming occurred at high southern latitudes (WAIS project members, 2010). This period was associated with a weakening of the Atlantic Meridional Ocean Circulation (AMOC), evidenced by Pa/Th in marine sediments (McManus et al., 2004; Ng et al., 2018). During the subsequent Bølling-Allerød (BA, ~14.7 to 12.8 ka) period, Greenland surface air temperatures rose by more than 10°C in just a few decades (Stephensen et al., 2008; Buizert et al., 2014), and the AMOC strengthened significantly (Severinghaus & Brook, 1999; McManus et al., 2004; Roberts et al., 2010; Ng et al., 2018). A cooling event at high southern latitudes, known as the Antarctic Cold Reversal (ACR), was identified between ~15 and 13 ka (Jouzel et al. 2007; Pedro et al., 2016), concurrent with the BA. The Younger-Dryas (YD, 12.8 to 11.7 ka) followed the BA, and was characterised by a drastic cooling in Greenland and the North Atlantic. While the processes leading to the YD are still debated (Renssen et al., 2015), it has been suggested that the YD could be attributed to a weakening of the AMOC (McManus et al., 2004), caused by a rerouting of freshwater into the Arctic that was then transported toward the deep-water formation sites of the

89 subpolar North Atlantic by coastal boundary currents (Condrón and Winsor, 2012; Kapsch et al., 2022).
90 Climate model simulations with marine proxy constraints support the variations in the AMOC during the
91 last deglaciation (Pöppelmeier et al., 2023).

92 An AMOC weakening causes a warming in the South Atlantic as the meridional oceanic heat
93 transport to the North Atlantic is weakened (Stocker & Johnsen, 2003; Stouffer et al., 2006). This
94 warming can then be propagated to the Southern Ocean and Antarctica (Pedro et al., 2018). The
95 contrasting temperature changes between Greenland and the southern high latitudes can also be found
96 during abrupt events of the last glacial period known as Dansgaard–Oeschger cycles (Dansgaard 1993;
97 NGRIP project members, 2004; WAIS Divide project members, 2015), which have led to the notion of a
98 bipolar seesaw (Stocker and Johnsen 2003; Capron et al., 2010). Alongside these events, the atmospheric
99 CO₂ increase throughout the deglaciation occurred in steps, suggesting a link ~~to~~with millennial-scale
100 climate events (Marcott et al., 2014) and changes in Southern Ocean circulation contributing to degassing
101 of oceanic carbon (Anderson et al., 2009; Menviel et al., 2018).

102 Transient climate simulations provide a suitable framework for assessing the processes leading to
103 deglacial climate changes. Early transient simulations that were conducted with transient orbital forcing,
104 GHGs and ice sheets suggested that an increase in austral spring insolation in the southern high latitudes
105 was responsible for the onset of warming (Timmermann et al., 2009), and that deglacial warming of the
106 Southern Ocean appeared as early as ~20 to 18 ka in association with sea ice retreat (Roche et al., 2011).
107 Transient simulations that also included freshwater input into the North Atlantic highlighted the AMOC
108 impact on climate change (Liu et al., 2009; He et al., 2011). Menviel et al. (2011) further showed that the
109 ACR could be a response to the strong AMOC increase at the end of HS1, but that its length and amplitude
110 could have been enhanced by meltwater input from the Antarctic ice sheet. These simulations were
111 designed to simulate AMOC changes in agreement with estimates from proxy records, and therefore the
112 magnitude, location, and timing of the implemented meltwater fluxes were idealised. In contrast,
113 experiments forced with meltwater fluxes consistent with ice sheet reconstructions based on sea-level
114 constraints often simulate millennial-scale AMOC changes in disagreement with accepted interpretations
115 of climate and ocean records (Snoll et al., 2024). Some experiments simulate an AMOC weakening at the
116 time of the BA because of significant mass loss of NH ice sheets (Bethke et al., 2012; Ivanovic et al.,

2018a; Kapsch et al., 2022; Bouttes et al., 2023) or do not simulate any abrupt climate events (Gregoire et al., 2012). With an idealised scenario that follows the evolution of NH ice sheets more closely (except for the 14 ka meltwater pulse), the MIROC climate model shows that it is possible to simulate an abrupt AMOC strengthening with the presence of continuous freshwater in the North Atlantic because of gradual warming (Obase and Abe-Ouchi, 2019). These studies indicate that different models have different sensitivities in terms of the AMOC response to forcing and, therefore, it is useful to analyse multi-model results for a robust understanding of the climatic processes.

To facilitate further examination of the mechanisms driving deglacial climate change, a protocol for carrying out transient simulations of the last deglaciation was proposed as part of the fourth phase of the Paleoclimate Modeling Intercomparison Project (PMIP4) (Ivanovic et al., 2016). The protocol of PMIP4 deglaciation summarised climate forcings needed (ice core based atmospheric GHGs and reconstructed ice sheets) for climate model experiments. The protocol is designed to be flexible in that the use of some boundary conditions is determined by each modelling group, which allows an exploration of different climate scenarios. The first PMIP multi-model study of the last deglaciation, focusing on the northern hemispheric climate during HS1, found that different freshwater approaches (*melt-uniform*, *melt-routed*, *trace-like*, *bespoke*, Snoll et al. (2024)) have a dominant impact on North Atlantic climate variability. While this finding could be drawn due to the flexibility of the PMIP deglaciation protocol (Ivanovic et al., 2016) regarding the choice of the method on how to distribute the freshwater forcing, this flexibility makes it challenging to properly compare the simulations. Nevertheless, the multi-model assessment of the last deglaciation performed here provides an opportunity to investigate the processes impacting southern high latitude climate and to evaluate the uncertainties from the models' sensitivity to the forcings.

Some boundary conditions for climate models, including GHG and Antarctic ice sheet (prescribed in PMIP4 protocol), result from climate change at high southern latitudes. Proxy records (Sigman et al., 2010, Skinner et al., 2010, Martinez-Garcia et al., 2011) and modelling studies (Bouttes et al., 2012, Menviel et al., 2016, Menviel et al., 2018, Gottschalk et al., 2019) indicate that physical and biogeochemical changes in the Southern Ocean may have significantly contributed to ocean carbon uptake during the last glacial period and to the atmospheric CO₂ increase during HS1. Subsurface warming on

145 the Antarctic shelf contributes to the mass loss of Antarctic ice sheets through enhanced melting of ice
146 shelves, and retreat of grounding lines (Golledge et al., 2014; Lowry et al., 2019). In addition, climate
147 conditions at high southern latitudes can impact the formation of Antarctic Bottom Water (AABW) and
148 the shoaling of AMOC (Sherriff-Tadano et al., 2023). Hence investigating the deglacial climate evolution
149 at high southern latitudes may give an insight into critical climate system feedbacks.

150 Here, we analyse the deglacial climatic evolution (21–11 ka) at high southern latitudes as
151 simulated in six PMIP4 transient experiments, and compare the results with paleo-proxy records. We
152 focus on the magnitude and rate of changes in Antarctic surface air temperature (SAT) and Southern
153 Ocean sea surface temperature (SST)-~~changes~~. As there is a substantial difference between the temporal
154 evolution of AMOC strengths in the simulations, we utilise statistical or simple models to separate the
155 impact of changes in atmospheric CO₂ and AMOC on Southern Ocean SST. Finally, we analyse the
156 evolution of the AABW, Southern Ocean westerlies and subsurface ocean temperature in the Southern
157 Ocean to discuss critical climate system feedbacks occurring at high southern latitudes.

158

159 2 Methods

160 2-1 Climate models and experiments used in this study

161 We use the PMIP4 transient simulations of the last deglaciation performed with six atmosphere-
162 ocean coupled climate models (Table 1), and analyse the time period from the LGM to the Early Holocene
163 21–11 ka. Table 2 summarises the experimental design of each model simulation and their reference
164 articles, with the evaluation of their LGM and PI states mentioned in their description. ~~These simulations~~
165 ~~are initialised with glacial conditions, and the~~ LGM climate fields (initial condition of these experiments)
166 have been evaluated by previous studies, particularly for global temperature changes (Kageyama et al.
167 2021), sea ice and SST changes in the Southern Ocean (Lhardy et al., 2021; Green et al. 2022), and SAT
168 changes over the Antarctic ice sheet (Buizert et al. 2021). A part of the transient simulations utilized in
169 this study have also been compared to proxy-reconstructions (Weitzel et al. 2024). Fig. S1 compares
170 simulated sea-ice edges for the pre-industrial simulations from six models used in this study, which shows
171 some models underestimate pre-industrial summer sea ice extent, but mostly to an acceptable level.
172 ~~simulate reasonable sea ice extents~~. The Equilibrium Climate Sensitivity (ECS, defined by global mean

173 SAT changes in response to doubling CO₂ from the pre-industrial) of each model ranges from 2.0 to
 174 3.9 °C, and the global mean surface air temperature (SAT) anomaly for the LGM is 3.5 to 7.3 °C (Table
 175 1). While some of the modelling groups performed two or more sensitivity experiments with different
 176 model parameters or boundary conditions (e.g., different freshwater forcing (FWF) scenarios or ice
 177 sheets), for this study we have selected one representative simulation from each climate model. Fig. 1
 178 summarises the time evolution of the climate forcings, i.e. insolation, atmospheric GHGs, and continental
 179 ice sheets used in the simulations. Both reconstructions (ICE-6G_C VM5a, henceforth ‘ICE-6G_C’; and
 180 ‘GLAC-1D’) have larger Antarctic ice sheet volume at the LGM, with a ~ 10 m sea-level equivalent
 181 volume change at the LGM, relative to present-day. Both suggest ~ 100 m of elevation ~~change-reduction~~
 182 since the LGM at EPICA Dome C (EDC, 123°E, 75°S), while WAIS Divide (WDC, 112°W, 79.5°S)
 183 differs by 300 m between the two datasets (Fig. 1d).

184 Fig. 2a summarises the total amount of FWF in the NH in six simulations. The FWF schemes can
 185 be classified into two groups: ~~:-{a}~~The first group with FWF adjusted to reproduce large-scale AMOC
 186 variability (iTRACE, LOVECLIM, MIROC), and ~~b}~~the second group with FWF consistent with the
 187 reconstructed ice volume changes (HadCM3, MPI-ESM, iLOVECLIM) based on ICE-6G_C or GLAC-
 188 1D (Fig. 2a, upper panel, red and black lines). Notably, during HS1, iTRACE and LOVECLIM have
 189 significant FWF (~ 0.2 Sv), while other simulations apply FWF of less than 0.1 Sv. In LOVECLIM and
 190 MIROC, the meltwater flux was uniformly applied to the North Atlantic, while other models use the
 191 location of the melting NH ice-sheet and associated runoff to apply a spatially varying FWF (Table 2).
 192 ICE-6G_C (HadCM3, MPI-ESM, iLOVECLIM) leads to a meltwater input of about 0.1 Sv to the
 193 Southern Ocean at 11.5–11 ka. iTRACE and LOVECLIM also applied freshwater flux to the Southern
 194 Ocean to simulate the ACR (iTRACE: up to 0.2Sv during 14.4–13.9 ka, LOVECLIM: fixed at 0.09Sv
 195 during 14.67–14.1 ka).

196 In section 3.3, we conduct further analysis to examine the processes driving Southern Ocean SST
 197 using a multilinear regression (MLR) model and a thermal bipolar seesaw model adapted from Stocker
 198 and Johnsen (2003).

200 2-2: Simple models to disentangle CO₂ and AMOC

2-2-1: Multilinear Regression model

We use a MLR model to regress changes in SST onto CO₂ and AMOC variations:

$$SST = \alpha_1 * CO_2 + \beta_1 * AMOC + \gamma, (1)$$

where *SST*, and *AMOC* (defined as the maximum meridional overturning streamfunction in the North Atlantic, at depths below 500 m and 20–60°N) are output from the climate models, and *CO₂* is the forcing used in each simulation. γ is the intercept. The AMOC in the analysis is normalised with respect to the temporal maximum and minimum values in each model. The CO₂ is also normalised with respect to the total change between 21 and 11 ka (~83 ppm). The MLR analysis is applied to the 2-D fields of the Southern Ocean SST. The same analysis is applied to the Southern Ocean SST averaged over 55–40°S. ~~Every~~ To focus on long-term climate change and reduce interannual variability, every 100-years, mean SST, AMOC, and CO₂ from 20 to 11 ka are used as the input for this analysis, so each dataset has 90 time-slices. While we use CO₂ as a representation of a gradual forcing as the input of the MLR model, we note that other forcing, such as from ice sheets and orbital changes can contribute to the warming. On the other hand, sensitivity experiments evaluating the contribution of each forcing show that they have a minor impact on Southern Ocean SST and Antarctic SAT changes between 19 and 15 ka (He et al. 2013). The results with coefficient of determination are displayed in Table 3.

2-2-2: Thermal bipolar seesaw model

As the MLR model does not consider transient climate response, we construct a thermal bipolar seesaw model following Stocker and Johnsen (2003). The original thermal bipolar seesaw model is based on an energy balance between the North and South Atlantic Oceans. We add the effect of CO₂ on temperature, which was not considered in the original model. The thermal bipolar seesaw model in this study solves the temporal evolution of Southern Ocean SST using the following equations:

$$\frac{d\Delta SST}{dt} = \frac{\Delta SST_{eq} - \Delta SST(t)}{\tau} (2)$$

$$\Delta SST_{eq} = \alpha_2 * CO_2(t) + \beta_2 * \textcolor{red}{AMOC}_m(t) (3)$$

where ΔSST_{eq} is an equilibrium Southern Ocean SST (change since the LGM) expected from the CO₂ and state of the AMOC at time t . $\Delta SST(t)$ is the SST change since LGM at time t , and τ is the characteristic timescale of the bipolar seesaw. $CO_2(t)$ is the CO₂ concentration at time t , and is normalised with maximum and minimum values as in the MLR model. The term $\textcolor{red}{AMOC}_m(t)$ represents the modes of the

書式を変更: フォント: 斜体

229 AMOC from the climate model outputs. When using the simulated AMOC within the bipolar seesaw
230 model, it is assumed that the AMOC ~~has only two~~ modes are binary, unlike the continuous values in the
231 model. Based on Figure 2, we assume that the AMOC is in a strong mode ($AMOC_m(t)=0$) if the AMOC
232 is greater than 14 Sv.

233 At first, we conduct systematic sensitivity experiments to calculate the minimum root mean square
234 error between the actual Δ SST and the bipolar seesaw models. We conduct 9610 sensitivity experiments
235 for each model within the parameter ranges shown in Table 43. The combination of parameters that gives
236 the minimum root mean square error, along with coefficient of determination between the climate models'
237 SST changes and bipolar seesaw models are displayed in Table 5.

239 3. Results

240 3-1: AMOC

241 As AMOC variations can impact southern high latitude climate, we summarise here the transient
242 evolution of the AMOC in the different simulations. As detailed below, the AMOC evolution is
243 substantially affected by the FWF schemes. All simulations except for MIROC display a strong (~20 Sv)
244 AMOC at the LGM (Fig. 2b), while MPI-ESM and iLOVECLIM shows slightly weaker LGM AMOC in
245 their sensitivity studies where ~~if~~ GLAC-1D ice sheet was used (Kapsch et al., 2022; Bouttes et al., 2023).
246 The more vigorous LGM AMOC compared to Pre-Industrial (PI) is in line with the majority of PMIP4
247 simulations (Kageyama et al., 2021), although it is not consistent with LGM reconstructions from multiple
248 marine tracers (Lynch-Stieglitz et al., 2007; Bohm et al., 2015; Menviel et al., 2016). During the period
249 corresponding to HS1, the AMOC stays weak in MIROC and ~~significantly-substantially~~ declines in the
250 iTRACE and LOVECLIM simulations, as meltwater is added into the North Atlantic. On the other hand,
251 in the other simulations, there is only a slight reduction in AMOC (~1 Sv) as the meltwater input into the
252 North Atlantic stays below 0.05 Sv. At the BA (~14.7 ka), three models exhibit an abrupt change from
253 weak to strong AMOC, triggered by a rapid reduction in FWF (iTRACE and LOVECLIM) or as a
254 response to the gradual background warming (MIROC). These simulations, featuring an AMOC
255 strengthening, broadly agree with marine proxy records (Fig. 2b black line). On the other hand, the other
256 three simulations (HadCM3, MPI-ESM, iLOVECLIM) display an AMOC weakening due to a ~~significant~~

書式を変更: フォント: 斜体

substantial increase in FWF originating from the ice sheet collapse associated with Meltwater Pulse 1a (Deschamps et al., 2012). During the Younger-Dryas (12.8–11.7 ka), iTRACE, LOVECLIM, and MIROC simulate a ~~weakened~~ AMOC ~~state compared to BA~~ decline, corresponding to an increase in FWF or an oscillatory nature of the AMOC in MIROC (Kuniyoshi et al., 2022). HadCM3 simulates a small but gradual AMOC reduction throughout the YD, while MPI-ESM exhibits multi-centennial AMOC variability. At 11 ka, the AMOC strength returns to a strong mode except for iLOVECLIM, which stays weak after the BA.

3-2-1: 21–18 ka (onset of warming) and 18–14.7 ka (HS1)

Fig. 3 summarises the simulated Antarctic SAT (Fig. 3c-d) and Southern Ocean SST (Fig. 3e) changes since the LGM in all the simulations (LGM is defined as 21 ka in most models, with some exceptions because of different initialisation; ~~20.6 ka for LOVECLIM~~, 20.0 ka for iTRACE, ~~20.6 ka for LOVECLIM~~). The SAT at WDC and EDC are compared with the ice core based reconstructions from Parrenin et al. (2013) and Buizert et al., (2021). Three models (MIROC, HadCM3, MPI-ESM) exhibit a gradual ~1°C warming between 21 and 18 ka at both WDC and EDC (Fig. 3c). This simulated EDC warming is comparable with ~~EDC~~ ice core estimates, with MPI-ESM overestimating the warming at the EDC site (Parrenin et al., 2013 Fig. 4a). However, the magnitude of warming suggested from WDC (~2°C warming between 19.5–19 ka, Shakun et al., 2012) is not fully simulated by any of the models, with iTRACE exhibiting slight cooling (Fig. 4a). MIROC, HadCM3 and MPI-ESM ~~also~~ simulate a significant SAT increase over Antarctica and ~~a~~ 0.5–1.0°C SST increase in the Southern Ocean north of the sea ice edge, with a gradual reduction in Southern Ocean sea ice area (Figs. 3f and 4b).

All models exhibit a larger warming between 18 and 14.7 ka (i.e. HS1) than between 21 and 18 ka. iTRACE simulates the largest warming in SAT at WDC and EDC (+6–8°C, Figs. 3c-d), closely following the estimates from ice core data. The sharp increase in temperature in iTRACE starts at ~18 ka, corresponding to a period of major reduction in AMOC strength (Fig. 3b). The warming in MPI-ESM follows iTRACE with a 5°C warming, despite a minor reduction in AMOC strength. The HadCM3 exhibits ~4°C warming at WDC and ~2°C warming at EDC, while the other models simulate a 2–4°C warming at EDC and WDC (Fig. 3c–d). iTRACE exhibits ~~the most significant~~ Southern Ocean SST

increase of 5 °C and LOVECLIM exhibits a sharp Southern Ocean SST increase of ~3°C, in response to an AMOC reduction at ~17 ka. The other models' Southern Ocean SST increase by 1–2 °C (Fig. 3e). Southern Ocean sea ice area exhibits the same trends as the Southern Ocean SST, with iTRACE simulating the largest sea ice area reduction of up to 40% compared to the LGM (Figs. 3f and 4b). Noting that iTRACE has the largest LGM sea ice extent (Fig. 4b).

3-2-2: 14.7–13 ka (BA) and 13–11 ka (YD and Holocene onset)

Three models (iTRACE, ~~MIROC~~, LOVECLIM, ~~MIROC~~) simulate an abrupt AMOC increase at the BA onset (Fig. 3b), and a concomitant cooling at high southern latitudes: ~1-2 °C Antarctic SAT and Southern Ocean SST decrease (Fig. 3c-e). iTRACE and LOVECLIM exhibit a sharp cooling in Southern Ocean SST and SAT in the early phase of the BA (Fig. 3e), probably enhanced by the meltwater flux into the Southern Ocean (Menviel et al., 2011). In contrast, the three other models (HadCM3, MPI-ESM, iLOVECLIM) exhibit a warming in the early phase of the BA, corresponding to an AMOC weakening. Subsequently, HadCM3 and MPI-ESM exhibit a gradual cooling over the Antarctic and Southern Ocean as the AMOC strengthens in the later part of the BA (~13.5 ka). iLOVECLIM displays a rapid warming at 13.5 ka, followed by a cooling-, which is explained by abrupt surface albedo changes caused by the evolving land-sea mask in the Antarctic region (Bouttes et al., 2023).

During YD (13–11ka), iTRACE, ~~LOVECLIM, and MIROC~~, ~~and LOVECLIM~~ simulate an AMOC weakening as well as a high southern latitude warming. iTRACE simulates a ~3–4°C increase in Southern Ocean SST, while LOVECLIM and MIROC simulate a 1°C warming. MPI-ESM exhibits multi-centennial variability associated with variations in AMOC strength. MPI-ESM and iLOVECLIM exhibit sharp cooling in Southern Ocean SST and SAT starting at ~11.5 ka, enhanced by the meltwater flux into the Southern Ocean (Kapsch et al., 2022).

The proxy-record based estimates on total deglacial (21–11 ka) warming is 10 °C in WDC, while the EDC estimates range from 5 to 10 °C (Parrenin et al., 2013; Buizert et al., 2021). Across the simulations, a 2 to 10 °C warming is simulated over Antarctica (Fig. 3c-d). In line with the WDC and the upper range of EDC estimates, iTRACE and MPI-ESM display a 8–10 °C total warming over Antarctica. Since the LGM, the Southern Ocean sea ice edge retreats poleward by 10° latitude in most models with the largest sea ice retreat (Fig. 5). A SST increase of up to 6 °C is simulated ~~in this area~~ in the Southern

Ocean near the winter sea ice edge in iTRACE, LOVECLIM, HadCM3, and MPI-ESM, while a ~4 °C SST increase is simulated in MIROC and iLOVECLIM (Fig. 5).

The different magnitudes of warming during HS1 and YD between models could be explained by the range of temperature changes between LGM and PI, as the mean SAT and SST changes are different by a factor of two (Table 1). To reduce this model difference, Antarctic SAT are normalised by the temperature anomaly between LGM and PI in Figure 6. When normalised, the simulations with a weak AMOC during HS1 show the largest warming over Antarctica (Fig. 6 left). The normalised Antarctic SAT change at 11 ka lies in between 0.6 and 0.8 with respect to the total temperature change between LGM and PI for five out of six models, indicating ~~This indicates that~~ additional warming is simulated between 11 and 0 ka in the model simulations. ~~occurred after the onset of the Holocene, which marks~~ ~~This is different~~ from ice core reconstructions, ~~between the simulations and proxy data,~~ in that the temperature at 11 ka is comparable to the pre-industrial values ~~based on ice core reconstructions~~ (Parrenin et al., 2013; Buizert et al., 2021).

3-3: SST – CO₂ – AMOC relationship analysis

The simulated AMOC time series display large differences across simulations due to different FWF ~~schemes~~ groups, which complicates the quantification of CO₂ forcing and AMOC changes in driving high southern latitude temperature changes in each model. To overcome this, we examine the Southern Ocean SST trajectory against CO₂ forcing, and AMOC strength (Fig. 7). Fig. 7 shows that the deglacial increase in atmospheric CO₂ has ~~major~~ significant impacts on the Southern Ocean SST because the temperature trajectory is mostly proportional to CO₂ changes unless there are ~~significant~~ major AMOC changes. Temperature changes associated with changes in AMOC are superimposed on Southern Ocean SSTs, in that ~~a~~ weaker AMOC compared to the long-term mean of respective models ~~weakening~~ (blue circles) tends to induce a warming, and vice versa. Even though the actual time series of AMOC in each model are very different, this result suggests that high southern latitude temperature changes can be decomposed into the effects of CO₂ and AMOC. The relative importance of CO₂ and AMOC are quantified in the following subsections.

3-4: Results of MLR and bipolar seesaw model

341 The results of the MLR model indicate that the CO₂ coefficients range from 1.0 to 6.5°C for the
342 total deglacial CO₂ changes (Table 34). All models have a negative coefficient of AMOC (−0.3 to −2.4°C),
343 indicating a Southern Ocean SST increase associated with an AMOC weakening. ~~The negative coefficient
344 of AMOC in all models suggest that an AMOC shutdown during HS1 has the potential to explain about
345 half of the SST changes.~~

346 The regression against Southern Ocean 2-D SST fields indicates that the CO₂ coefficient is mostly positive
347 over the Southern Ocean, ranging from ~0.5 °C in the Antarctic zone where sea ice is present until 11 ka,
348 to 2–6 °C in the Southern Ocean north of the LGM winter sea ice edge (Fig. 8). The sensitivity to the
349 AMOC is mostly negative in the Southern Ocean, and areas of high sensitivity overlap with those of CO₂,
350 suggesting sea ice modulates the areas sensitive to both CO₂ and AMOC changes.

351 3-5: Results of bipolar seesaw model

352 Table 5 summarises the results of the bipolar seesaw model. All models have positive CO₂
353 coefficients (2.0–6.0°C) and negative AMOC coefficients (−0.5 to −2.9°C), as in the MLR models. The
354 time series simulated by the bipolar seesaw model are compared with actual SST changes and with MLR
355 models in Fig. 9. The bipolar seesaw model succeeds in reproducing a gradual SST decrease as a result
356 of an AMOC strengthening (e.g. gradual cooling in iTRACE and MIROC, 15–13 ka). This gradual
357 cooling was not represented by the MLR model, which exhibits an immediate SST response to AMOC
358 changes. The response time ranges from 100–700 years, with most models ranging from 500–700 years
359 with the exception of LOVECLIM and iLOVECLIM (Table 5). We also applied the bipolar seesaw model
360 by using AMOC and CO₂ coefficients from six different models (Table 5), but common inputs of CO₂
361 (Bereiter et al., 2015) and AMOC from iTRACE. The results indicate that all models would have
362 simulated a cooling at the surface of the Southern Ocean during BA if there was an increase in the AMOC
363 at the beginning of BA as simulated in iTRACE, LOVECLIM or MIROC (Fig. S2).

364 We note that the values of the CO₂ sensitivity from the MLR and bipolar seesaw model may
365 include gradual forcing from other greenhouse gases, ice sheets, and orbital forcing. In addition, a sharp
366 cooling associated with freshwater in the Antarctic Ocean was not represented because both models, MLR
367 and bipolar seesaw, do not consider meltwater in the Southern hemisphere (~14.5 ka of iTRACE and
368 LOVECLIM, ~11.5 ka of MPI-ESM and iLOVECLIM)

書式変更: インデント: 最初の行: 0 mm

書式を変更: 下付き

書式を変更: 下付き

369

370 **3-65: Other Southern Ocean climate variables**

371 We further analyse AABW transport (minimum global meridional overturning streamfunction, at
 372 depths below 3000 m and 60°S–30°S) as an indicator of Southern Ocean meridional circulation, and 850
 373 hPa zonal mean winds over the Southern Ocean (zonal mean winds averaged over 65°S–40°S). to discuss
 374 potential impact on deglacial CO₂ changes, which is prescribed in the experiments. We focus on the onset
 375 of deglaciation (21–18 ka) and the initial significant increase in CO₂ (~HS1, 18–15 ka). The AABW (Fig.
 376 10b) at the LGM ranges from 10 to 30 Sv among the six models and stays relatively constant between 21
 377 and 18 ka. In the subsequent period (18–15 ka), iTRACE exhibits a significant gradual decline in the
 378 AABW, in phase with Southern Ocean SST changes (Fig. 10d). LOVECLIM and MPI-ESM exhibit a
 379 gradual decline in AABW (~5 Sv), while three other models (MIROC, HadCM3, iLOVECLIM) exhibit
 380 a small reduction or a stable AABW. Thus, while all models simulate Southern Ocean SST warming and
 381 sea ice retreat during HS1, the trends in AABW differ. In addition, the AABW changes do not depend on
 382 the AMOC evolution and thus FWF groups (Fig 10a–b). The zonal winds over the Southern Ocean exhibit
 383 slight do not change significantly change between 21 and 18 ka, apart in from MIROC and MPI-ESM,
 384 which exhibit a slight weakening (Fig. 10c). Between 18 and 15 ka, the zonal winds continue to decline
 385 in MIROC and MPI-ESM, and start to decline in iTRACE and LOVECLIM. Little changes in zonal winds
 386 are simulated in iLOVECLIM, while HadCM3 exhibits a ~10% strengthening.

387 Subsurface ocean temperatures south of 60°S at depths of around 500 m (Fig. 10e) exhibit an
 388 increase during HS1 in 4 of the 6 simulations, with the largest warming (1.2 °C and 0.8 °C) simulated by
 389 the two simulations which exhibited the largest SST increase (iTRACE and MPI-ESM). During the ~~ACR~~
 390 BA (15–13 ka), iTRACE and MIROC exhibit a gradual sub-surface temperature decrease while HadCM3
 391 and MPI-ESM exhibit a continuous warming, as per the SST changes in the respective models.
 392 iLOVECLIM and LOVECLIM exhibit small changes (<0.5°C) in the total sub-surface temperature.
 393 Abrupt subsurface warming in iTRACE (~14 ka) and LOVECLIM (14.8–14.2 ka) coincide with Southern
 394 Ocean SST reduction, suggesting that this results from enhanced Southern Ocean stratification as a
 395 response to Southern Ocean meltwater input (Menviel et al., 2011; Lowry et al., 2018).

396 **3-76: Additional freshwater experiments on HS1 SO warming in MIROC and HadCM3**

書式を変更: 下付き

We additionally show two simulations run with the MIROC and HadCM3 models to assess the impact of FWF on southern high latitude climate ~~of a significant AMOC decrease~~ during HS1. We remind that the MIROC and HadCM3 comes from different freshwater groups (Fig. 2). In the MIROC simulations, the FWF during HS1 is increased to 0.1 Sv or 0.2 Sv between 18 and 15.5 ka (Figure 11a, red and orange lines) instead of 0.03 Sv in the standard simulation. This larger meltwater input further weakens the AMOC (Fig. ~~ure~~ 11a) and leads to an additional 1 °C SST increase in the SO compared to the standard simulation (Fig. 11d). The 1 °C warming in response to AMOC reduction of ~5 Sv is ~~significantly~~ higher than results from the MLR and bipolar seesaw models. In the HadCM3 simulations, a North Atlantic freshwater flux of ~0.2 Sv during HS1 (similar to Trace-21ka A, Liu et al., 2009) ~~significantly~~ reduces the AMOC by 15 Sv (Fig. ~~ure~~ 11~~be~~ blue lines), and induces an additional ~1 °C increase in Southern Ocean SST compared to the standard simulation (Fig. 11h). The simulated HS1 warming in HadCM3 is consistent with both MLR and bipolar seesaw models (Tables 3 and 5). The results from the MIROC and HadCM3 sensitivity experiments show that the simulated warming during HS1 can be twice as strong with an AMOC shutdown compared to the standard simulation of each model. As in the LOVECLIM Heinrich stadial 4 simulation (Figure S2; Margari et al. 2020) the warming in the southern high latitude in response to AMOC strength is not necessarily linear, while MLR models assume a linear temperature response to the AMOC.

4. Discussion

4-1: Onset of deglacial warming

The climate forcing in the early deglaciation primarily comes from insolation due to obliquity and precession changes (Fig. 1a), which leads to an increase in spring to summer insolation south of 60 °S (Fig. S23). Ice core data suggest that the onset of deglacial warming at WDC was earlier than the increase in CO₂, and this early deglacial warming has been suggested to result from an AMOC reduction (Shakun et al., 2012) or local insolation changes (WAIS project members, 2013). However, simulated early warming is smaller than proxy records. Three models (MIROC, HadCM3, MPI-ESM) exhibit a small but ~~significant~~ warming (~ 0.5°C) between 21 and 18 ka (Fig. 4a) in both West and East Antarctica, as well

423 as at the surface of the Southern Ocean, primarily in the Pacific sector (Fig. 4b) as suggested by proxy
424 records (Moy et al., 2019; Sikes et al., 2019; Moros et al., 2021). The amplitude of the early warming in
425 these models is comparable to a previous modelling study (Timmermann et al., 2009), while the other
426 models show a slight cooling (iTRACE) or little change (LOVECLIM and iLOVECLIM).

427 The first explanation for the differences in the simulated temperature change between 21 and 18
428 ka is the Southern Ocean sea ice at LGM. MIROC, HadCM3 and MPI-ESM have less LGM summer sea
429 ice than other models. The smaller sea ice extent at the LGM, relative to other models, may lead to a high
430 sensitivity to increased insolation during austral spring to summer, causing significant warming with sea
431 ice retreat (Timmermann et al., 2009; Roche et al., 2011). If the LGM Southern Ocean sea ice extent is
432 extensive, the increase in insolation primarily south of 60 °S (Fig. S23) does not warm the Southern Ocean
433 as much because of high sea ice albedo. Although the local insolation changes are the likely cause of an
434 early warming simulated in some of the models, the addition of freshwater could contribute to the AMOC
435 weakening. For example, the consideration of an additional freshwater flux from the Fennoscandian ice
436 sheet in the freshwater forcing prior to 18 ka as included in MPI and as suggested by Toucanne et al.
437 (2010), would weaken the AMOC and lead to a more pronounced warming in the southern high latitudes.

438 Another model-data difference is the different early warming rates between West and East
439 Antarctica. The data from WDC suggest there was significant warming in West Antarctica, while a less
440 significant change in East Antarctica is suggested by EDC. In contrast, the models simulate similar
441 warming rates in both West and East Antarctica (Fig. 4a), suggesting the models may underestimate the
442 spatial heterogeneity in West and East Antarctic warming. This might be attributed to the Antarctic ice
443 sheet history prescribed in the experiments, where both ICE-6G_C and GLAC-1D have minor surface
444 elevation changes at WDC in the early deglaciation (Fig. 1d). Buizert et al. (2021) used the MIROC and
445 HadCM3 models and showed that the uncertainty in Antarctic ice sheet height affects the difference
446 between LGM and PI temperatures because changes in surface elevation affect SAT (~1 °C warming per
447 100 m altitude reduction). This might suggest that the lower surface elevations at WDC, related to the ice
448 sheet terminus retreat between 20–15 ka in the Amundsen Sea (Bentley et al. 2014), may have contributed
449 to the early deglacial warming primarily in West Antarctica. The coarse resolution of the atmospheric
450 models (2.5 to 5.6 degrees in the horizontal) may impact the warming contrast between East Antarctica

(EDC ice core site)IS and West Antarctica (WDC ice core site)IS through an inherent smoothing of the surface topography of the Antarctic ice sheet and the associated impact on the atmospheric circulation (Buizert et al., 2021). In addition, the relatively coarse resolution of the ocean models (1 to 3 degrees), may impact the AMOC sensitivity to iceberg and freshwater flux in the North Atlantic (Condrón and Winsor 2012), or parameterizations the impact of mesoscale processes in the Southern Ocean (Morrison et al., 2013) and their response to the deglaciation.

Uncertainty in the Antarctic ice sheet topography could also explain some model-data differences during the early Holocene, where simulations indicate that an additional warming occurs after the onset of the Holocene 11 ka (Fig. 6). This is different from ice core data (Fig. 4) and global mean ocean temperature (including deep-sea temperature) estimated from noble gases in ice cores, which suggests that temperatures reach Holocene levels at the end of YD (Bereiter et al., 2018). The higher-decrease in surface elevation of the Antarctic ice sheet at after 11 ka compared to the present day in the experimental design (Fig. 1e) may contribute to the simulated Holocene warming. It would be valuable to assess the uncertainties from ice sheet reconstructions, as new reconstructions have been published (e.g., Gowan et al., 2021), and different LGM ice sheets can induce different AMOC variabilities (Prange et al., 2023; Masoum et al., 2024).

4-2: Rate of temperature changes

HS1 (~18–14.7 ka) exhibits significant-major warming in all models because of the CO₂ increase, with the total warming being dependent on the sensitivity of each model to CO₂ and to AMOC changes. In turn, the deglacial AMOC evolution is dictated by the glacial meltwater input, as shown in additional sensitivity experiments performed with MIROC and HadCM3 (Fig. 11). iTRACE simulates the largest warming during HS1 among six models, with an Antarctic SAT increase of 6–8°C and Southern Ocean SST of 4–5°C. While the Antarctic SAT matches ice-core data, Southern Ocean SST is larger than the SST stack. Five models besides iTRACE simulate a Southern Ocean SST change which compare well with the SST stack data, but these five models underestimate Antarctic SAT. This indicates that the different magnitudes of warming between Southern Ocean SST and Antarctic SAT are weakly simulated not fully represented in models. While iTRACE exhibits the largest cooling of global mean SAT changes at the LGM compared to PI (7.3 °C, compared to the six-model mean of 5.3 °C), the ECS of

iTRACE (3.6 °C) is not the highest among the six models; instead, MIROC4m has the highest ECS despite weaker deglacial warming (Table 1). We examine the relationship between ECS and the LGM global mean SAT changes using multi-model PMIP3 and PMIP4 simulations (Fig. S43). We find a weak negative correlation (−0.06) between the ECS and global mean LGM SAT changes, and the local SAT change in the individual climate models can vary by about a factor of two even with the same ECS. A substantial asymmetry between warm and cold climates has been identified in previous studies because of the presence of continental ice sheets, ocean dynamics, and cloud feedback (Yoshimori et al., 2009; Zhu and Poulsen, 2021). Hence, understanding the mechanism and amplitude of cooling in the LGM simulations will contribute to a better understanding of multi-model differences in the deglacial warming.

The sensitivity to AMOC ranges between (−0.5 to −2.9°C) based on the analysis using the thermal bipolar seesaw model (Table 5). A multi-model study comparing freshwater hosing experiments of 11 climate models (including LOVECLIM, MIROC, and HadCM3 used in this study) under LGM climate shows that most models exhibit warming in the Southern Ocean (Kageyama et al., 2013). However, the simulation length in their study is less than 420 years. In this study, we as opposed to the estimated the timescale for the bipolar seesaw to be in this study (~500–700 years), suggesting the need for Thus, longer simulations are needed to evaluate the extent of the climate response at high southern latitudes.

The MLR and thermal bipolar seesaw models in this study include several assumptions. Firstly, as the gradual forcing is represented only by the CO₂ concentration, they do not consider the effect from retreating ice sheets, meltwater flux in the Southern Ocean, or insolation changes explicitly. Other forcings besides CO₂ and AMOC, could be included in the CO₂ or AMOC coefficients in this analysis. For instance, other gradual forcings insolation change in Northern summer have positive correlations with the CO₂ forcing because both exhibit gradual increase (Fig. 1a-b). Antarctic and Northern Hemisphere ice sheet changes could impact Southern Ocean SST (Abe-Ouchi et al., 2015) through deep-water formation. This may explain the CO₂ coefficients from the MLR and bipolar seesaw model that are higher than expected from the ECS value. On the other hand, the AMOC sensitivity of the LOVECLIM model is low compared to the 1.5 °C Southern Ocean SST increase found in the simulation of Heinrich stadial 4 (Margari et al. 2020, Fig. S54), and the CO₂ coefficient is quite high, potentially implying a poor separations of the two factors.

4-3: Freshwater forcing and temperature changes in southern high latitudes

As shown here, the deglacial AMOC variations are quite different amongst the simulations. Only those which display an AMOC increase at the end of HS1 can capture a cooling trend at BA (corresponding to the ACR) as suggested by ice-core data (iTRACE, LOVECLIM, MIROC). In comparison to previous transient simulations of the last deglaciation, the representation of the duration of the ACR has improved, as it was previously simulated as too short (Lowry et al., 2018). On the other hand, individual climate model simulations that are forced with a large NH meltwater pulse consistent with ice sheet reconstructions do not simulate ~~an ACR~~ an increase in the AMOC at the BA (Ivanovic et al., 2016; 2018; Kapsch et al., 2022; Bouttes et al., 2023). FWF in the NH and associated reduction in the AMOC lead to Antarctic warming during HS1 in the sensitivity experiments with individual forcing (He et al., 2013) and sensitivity experiments with FWF (Figure 11). A comparison of the six models reveals that capturing phase changes in the AMOC is necessary to simulate warming or cooling trends at southern high latitudes. This is also supported by results of the bipolar seesaw models forced with a common AMOC (Fig. S2). While MIROC simulates a rapid increase in the AMOC at BA transition with a continuous freshwater flux (Fig. 2), a greater FWF by a factor of 1.5 leads to a weak AMOC throughout the last deglaciation (Obase et al., 2021). Thus, the simulated temperature changes at southern high latitudes are sensitive to FWF in the NH. However, the timing and magnitude of meltwater input inferred from ice sheet reconstructions is still different from meltwater needed to obtain a deglacial climate evolution in agreement with proxy records. This-This so-calledso-called meltwater paradox (Ivanovic et al., 2018; Snoll et al., 2024) is present for a major periods of the last deglaciation including the BA transition and HS1, suggesting a need for a better assessment of freshwater scenarios, and the-potentiala need to assess the sensitivity of climate models to freshwater forcing, and the necessity to reduce potential climate model biases. We also note that the routing location of meltwater input (Roche et al., 2010; He et al., 2020) and the consideration of icebergs and meltwater discharge into the ocean (Schloesser et al., 2019; Love et al., 2021) may induce quite-different AMOC changes. -In addition, FWF from the Antarctic ice sheetSouthern FWF can enhance the ACR, as found in iTRACE (~14.2 ka) and LOVECLIM (~14.7 ka), with a sharp cooling in Southern Ocean SST and Antarctic SAT primarily in WDC. This is caused by the intensified stratification in the Southern Ocean (Meniel et al., 2010; 2011), which induces

書式を変更: フォント: 太字

書式を変更: フォント: 太字

書式変更: インデント: 最初の行: 0 mm

535 significant warming in the subsurface and contributes to further mass loss from Antarctic ice sheets
536 (Golledge et al., 2014). As ice core data does not exhibit such sharp cooling events as compared to climate
537 model simulations (Fig. 3), this may provide some constraints on the extent and duration of FWF from
538 the Antarctic ice sheet. ▲

書式を変更: フォント: (日) + 本文のフォント - 日本語 (MS 明朝), (言語 1) 日本語

540 **4-34: Implications for climate system changes at high southern latitudes**

541 Reconstructions have suggested that changes in Southern Ocean circulation, probably driven by
542 wind changes, were important for the modulation of Southern Ocean CO₂ outgassing during the
543 deglaciation. Proxies suggest an enhanced opal flux during HS1, which could reflect increased upwelling
544 in the Southern Ocean due to changes in Southern Hemispheric westerlies (SHW) (Anderson et al., 2009),
545 and poleward shift of the SHW across the deglaciation (Gray et al., 2023). Proxies also suggest decreasing
546 deep and intermediate-depth Southern Ocean ventilation ages (Skinner et al., 2010, Burke et al., 2011),
547 increasing intermediate-depth pH in the Southern Ocean during HS1 (Rae et al., 2018). It has been
548 suggested that stronger or poleward-shifted SHW and/or enhanced AABW formation during HS1 would
549 indeed enhance Southern Ocean CO₂ outgassing and lead to an atmospheric CO₂ increase (Menviel et al.,
550 2014; Menviel et al., 2018). In contrast, in the present study, most models show very little change or a
551 gradual weakening in the SHW across the deglaciation, and there is little latitudinal migration of the SHW.
552 Only the HadCM3 model displays a SHW strengthening during HS1. Biases in the SHW in PI simulations
553 can be a cause of little changes in SHW. However, additional studies should look in more details into
554 potential changes in the ~~location of the~~ SHW in these simulations, as well as regional changes in SHW
555 strength and their relation to other climatic variables (Rojas et al., 2009; Sime et al., 2013). In addition,
556 no model exhibits an increase in AABW formation, which could contribute to the upwelling of carbon-
557 rich waters ~~mass in the deep ocean~~ and CO₂ outgassing from the Southern Ocean. Instead, the ~~deglaciation~~
558 ~~may have contributed to the~~ long-term AABW weakening ~~in AABW~~ by ~~warming the~~ Southern Ocean
559 ~~warming and enhancing~~ sea ice melt ~~, and decreasing surface salinity~~ are consistent with previous analysis
560 of deglaciation experiments (Marson et al., 2016). While it has been suggested that larger Southern Ocean
561 sea ice extent would lead to an atmospheric CO₂ decrease at the LGM (Ferrari et al., 2014; Marzocchi et
562 al., 2020, Stein et al., 2020), few models simulate significant changes in ~~oceanic~~ atmospheric CO₂ due to

563 ~~a~~-Southern Ocean sea ice change (Gottschalk et al., 2019). These physical changes still need to be
564 reconciled with processes put forward to explain the deglacial atmospheric CO₂ changes by running
565 coupled climate-carbon simulations.

566 Finally, we also find that changes in subsurface ocean temperature in the Southern Ocean, one of
567 the critical factors impacting the retreat of the Antarctic ice sheet, display significant differences across
568 the simulations. This could be related to different ECS or FWF in the Southern Ocean, and should also
569 be investigated in future studies to quantify uncertainties in subsurface ocean temperature changes.
570 Model-dependent subsurface ocean temperature change is one source of uncertainty in projecting future
571 Antarctic ice sheet mass loss (Serrousi et al., 2020). In contrast to the present simulations of the last
572 deglaciation, which prescribe the Antarctic ice sheet history, climate variability occurring during the
573 deglaciation can impact the Antarctic ice sheet, which can act as feedback to Southern Ocean climate via
574 meltwater input from the Antarctic ice sheet (Menviel et al., 2010; Golledge et al., 2014; Clark et al.,
575 2020). Hence, further coupled climate and ice sheet modelling studies are needed to improve our
576 understanding of climatological and glaciological processes and to evaluate model performance under a
577 warming climate and rising sea levels (Gomez et al., 2020).

578 5. Conclusion

579 In our multi-model analysis of transient deglacial experiments, the early increase in Antarctic SAT
580 is weakly simulated or absent. The multi-model difference could be related to ~~the smaller differences in~~
581 LGM sea ice extent, which may affect the sensitivity to insolation change, or to a slight reduction in the
582 AMOC in response to small freshwater input from NH ice sheets. In addition, the different warming rates
583 between West and East Antarctica suggested by ice core records are not reproduced by the transient
584 simulations. In all models, a major- warming occurs ~~at southern high latitudes~~ between 18 and 15 ka in
585 response to increased CO₂ concentration. The multi-model analysis and sensitivity experiments further
586 suggest that the AMOC reduction during HS1 associated with increased freshwater flux in the North
587 Atlantic contributes to a larger warming ~~in southern high latitudes~~, in agreement with high southern
588 latitude proxy records, even though no simulation can reproduce both the amplitude of Southern Ocean
589 SST and Antarctic SAT changes simultaneously. The bipolar seesaw model indicates ~~that~~ all models have
590 ~~a~~ bipolar seesaw response, and ~~that~~ an abrupt AMOC increase at the end of HS1 is necessary to simulate

the high southern latitude cooling during the BA (corresponding to the ACR). The simulations ~~do not~~ exhibit significant little changes in winds over the Southern Ocean ~~or~~ and meridional circulation in the Southern Ocean, thus questioning the processes that could have which could contributed to enhanced CO₂ outgassing from the Southern Ocean. This indicates the necessity for future climate system modelling studies to quantify the sequence of deglacial climate changes and atmospheric CO₂ increase.

Acknowledgements:

We thank the two anonymous referees for their valuable comments which have substantially improved our paper. TO, AAO, TV and WLC acknowledge funding from JSPS Kakenhi 17H06104, 17H06323, and JPJSBP120213203. TO was also supported by JPMXD0722680395 and JSPS ~~K~~kakenhi 24H00026. We acknowledge discussions at PAGES-QUIGS T5–T0 workshops, supported by INQUA Terminations Five to Zero (T5–T0) Working Group (Project #2004). LM acknowledges funding from Australian Research Council (ARC) grants FT180100606 and SR200100008. UM and MK acknowledge funding by the German Federal Ministry of Education and Research as a Research for Sustainability Initiative through the PalMod project (grant nos. 01LP1915C, and 01LP1917B). The MLR analysis used scikit-learn library of Python 3.7. The figures were created using Generic Mapping Tool (GMT version 4 and 6).

Data availability:

All model data supporting our findings will be archived at Zenodo. Original model data is upon request for authors from each modelling group.

Code availability:

The bipolar seesaw model and the MLR model used in this study can be shared upon request.

Author contribution:

TO, LM, and AAO conceived the study. TO, LM, TV, BS analysed the data. TO, LM, AAO, TV, RI, and BS wrote the manuscript with input from all co-authors.

Competing interests:

618 Laurie Menviel is a member of the editorial board of Climate of the Past, but otherwise all authors
619 declare that they have no conflict of interest.

620 **References:**

Name	Climate model name	<u>Equilibriu</u> <u>m Climate</u> <u>Sensitivity</u> <u>(ECS)</u> [K]	Global mean LGM SAT anomaly [K]	References
iTRACE	iCESM1.3	3.6	7.3	Tierney et al., (2020)
LOVECLIM	LOVECLIM	2.8	4.2	McDougall et al., (2020), Goosse et al., (2010)
MIROC	MIROC4m	3.9	4.5	Chan and Abe-Ouchi, (2020)
HadCM3	HadCM3B	2.7	6.1	Kageyama et al., (2021)
MPI-ESM	MPI-ESM-CR P2		6.1	<u>Kapsch et al., (2022)</u>
iLOVECLIM	iLOVECLIM	2.0	3.5	<u>Bouttes et al., (2023)</u>

621 **Table 1:** Summary of climate models analysed in this study. Note that the ECS for MPI-ESM (model
622 version MPI-ESM-CR P2) has not been calculated.

623

Name	Freshwater scheme	GHGs	Ice sheets	References for deglaciation experiments
iTRACE	TraCE-like	PMIP4	ICE-6G_C	He et al., 2019; 2021
LOVECLIM	TraCE-like, <u>spatially uniform to the North Atlantic</u>	Kohler et al., 2017	ICE-5G	Menviel et al., 2011
MIROC	ICE-6G_C with adjustment, <u>spatially uniform to the North Atlantic</u>	PMIP4	ICE-5G (LGM fix)	Obase and Abe-Ouchi 2019; Obase et al., 2021

書式を変更: フォント:(日)+本文のフォント- 日本語 (MS 明朝), (言語 1) 日本語

書式を変更: フォント:(日)+本文のフォント- 日本語 (MS 明朝), (言語 1) 日本語

書式を変更: フォント:(日)+本文のフォント- 日本語 (MS 明朝), (言語 1) 日本語

書式を変更: フォント:(日)+本文のフォント- 日本語 (MS 明朝), (言語 1) 日本語

624
625
626
627

HadCM3	ICE-6G_C	PMIP4	Ice-6G_C	Ivanovic et al., 2018; Snoll et al., 2022
MPI-ESM	ICE-6G_C	Kohler et al., 2017	Ice-6G_eC _A	Kapsch et al., 2022
iLOVECLIM	ICE-6G_C	PMIP4	Ice-6G_eC _A	Bouttes et al., 2023

Table 2: Summary of the experimental design used in the transient deglacial simulations. **PMIP4 in the column GHGs indicates they use three GHGs reconstructions (CO₂, CH₄, N₂O) in PMIP4 protocol paper (Ivanovic et al., 2016).**

Parameter [unit]	Range
CO₂ coefficient α [K/83 ppm]	1.0–7.0, every 0.2
AMOC coefficient β [K/(normalised AMOC)]	0.0–3.0, every 0.1
Response timescale τ [year]	100–1000, every 100

~~**Table 3:** Parameter ranges in the thermal bipolar seesaw model.~~

	CO ₂ coefficient [K/83 ppm]	AMOC coefficient [K/(normalised AMOC)]	Coefficient of Determination
iTRACE	6.5	−2.4	0.90
LOVECLIM	4.1	−0.4	0.91
MIROC	1.4	−0.5	0.81
HadCM3	3.3	−1.4	0.95
MPI-ESM	3.1	−1.2	0.90
iLOVECLIM	1.0	−1.4	0.56

Table 34: Results of the MLR model for Southern Ocean SST.

Parameter [unit]	Range
CO ₂ coefficient α [K/83 ppm]	1.0–7.0, every 0.2
AMOC coefficient β [K/(normalised AMOC)]	0.0–3.0, every 0.1

- 書式を変更: フォント:(日)+本文のフォント- 日本語 (MS 明朝), (言語 1) 日本語
- 書式を変更: フォント:(日)+本文のフォント- 日本語 (MS 明朝), (言語 1) 日本語
- 書式を変更: 下付き
- 書式を変更: 下付き
- 書式を変更: 下付き
- 書式を変更: フォント:(日)+本文のフォント- 日本語 (MS 明朝), (言語 1) 日本語

629

630

Response timescale τ [year] 100–1000, every 100

Table 43: Parameter ranges in the thermal bipolar seesaw model.

	CO ₂ coefficient [K/83 ppm]	AMOC coefficient [K/(normalised AMOC)]	Response timescale [year]	Coefficient of determination
iTRACE	6.0	−2.9	500	0.97
LOVECLIM	4.4	−0.6	300	0.94
MIROC	2.4	−0.9	600	0.97
HadCM3	4.8	−1.3	700	0.99
MPI-ESM	3.4	−1.4	500	0.95
iLOVECLIM	2.0	−0.8	100	0.54

631

Table 5: Results of the bipolar seesaw model for Southern Ocean SST

書式を変更: フォント:(日)+本文のフォント-日本語 (MS 明朝),(言語 1) 日本語

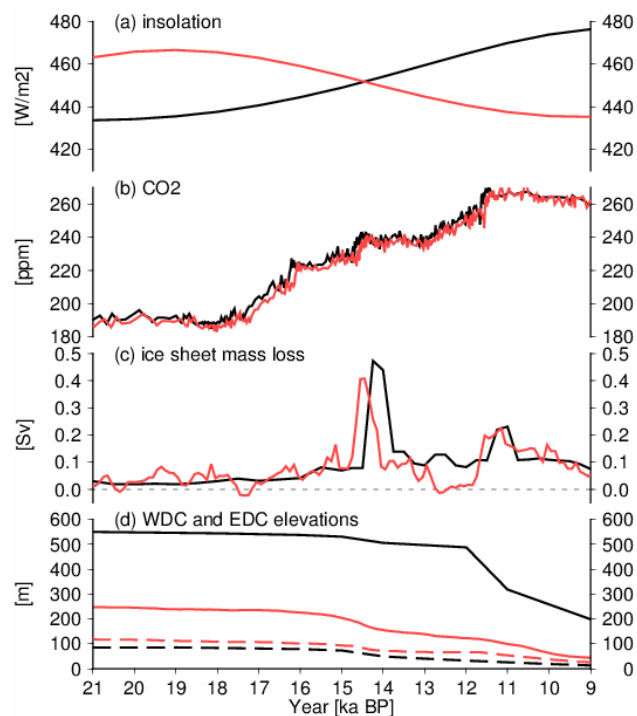


Figure 1: Forcing of the last deglaciation. (a) Insolation based on Berger (1978). Black: 65°N July, red: 65°S January based on Berger (1978), (b) CO₂. Black: Bereiter et al., (2015), red: Kohler et al., (2017), (c) FWF in the NH from ICE-6G_C (black lines) and GLAC-1D (red lines), (d-e) Elevation change at WDC (bold lines) and EDC (dashed lines) from ICE-6G_C (black lines) and GLAC-1D (red lines).

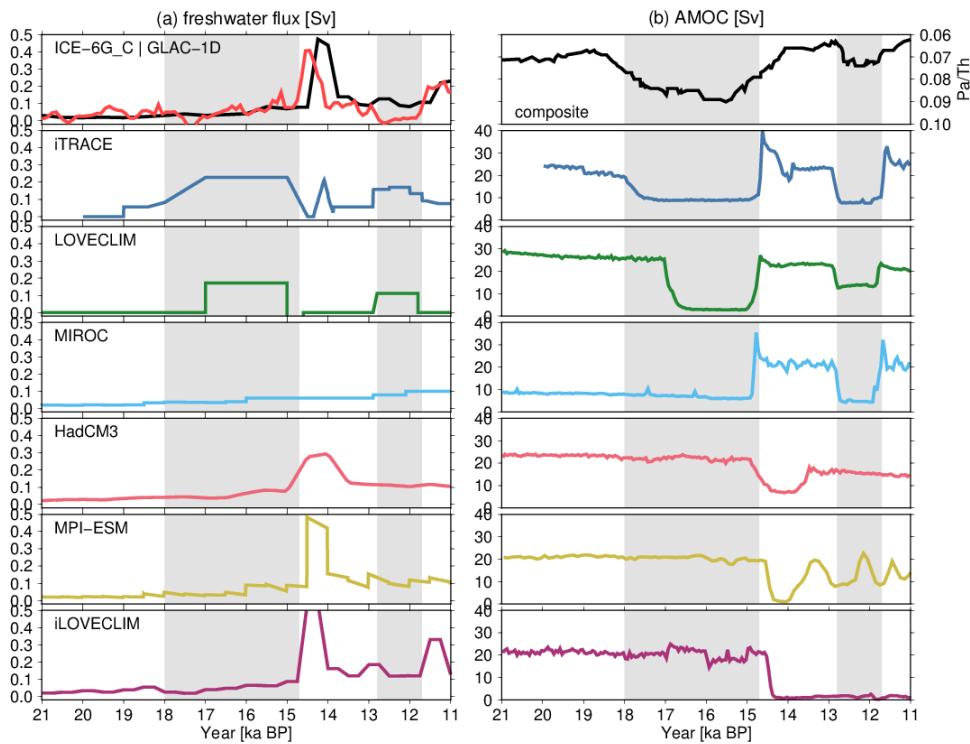


Figure 2: (a) Freshwater forcing (total value in the NH) and (b) simulated AMOC time series. The top panels indicate the freshwater flux from ice sheet reconstructions (black indicates ICE-6G_C and red indicates GLAC-1D) and composite $^{231}\text{Pa}/^{230}\text{Th}$ in the North Atlantic, retrieved from Ng et al., (2018). The top three model panels correspond to the first group with FWF adjusted to reproduce large-scale AMOC variability, and the bottom three model panels correspond to the second group with FWF consistent with the reconstructed ice volume changes. The grey shading indicates HS1 (18–14.7 ka) and the YD (12.8–11.7 ka), respectively, and the period in between corresponds to the BA (14.7–12.8 ka).

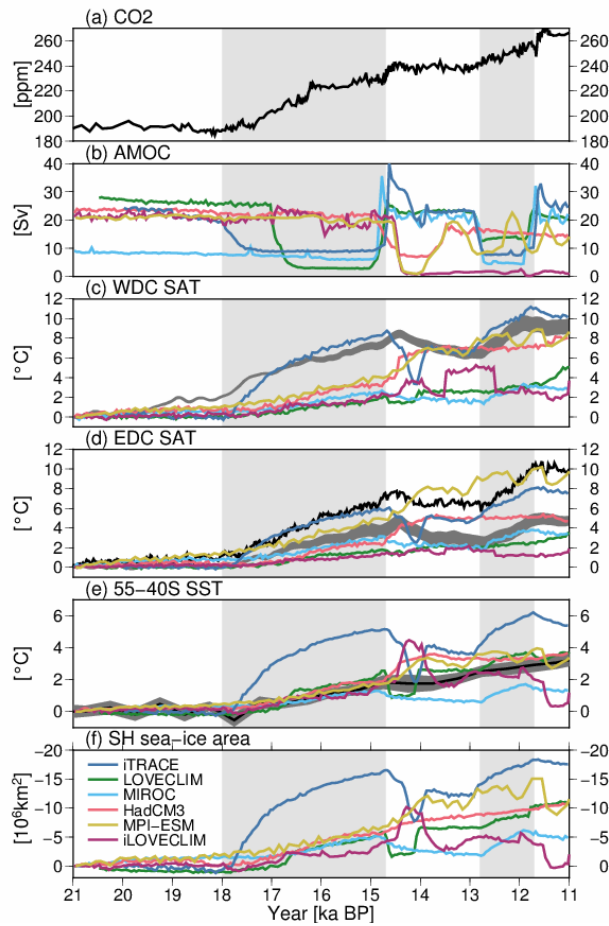
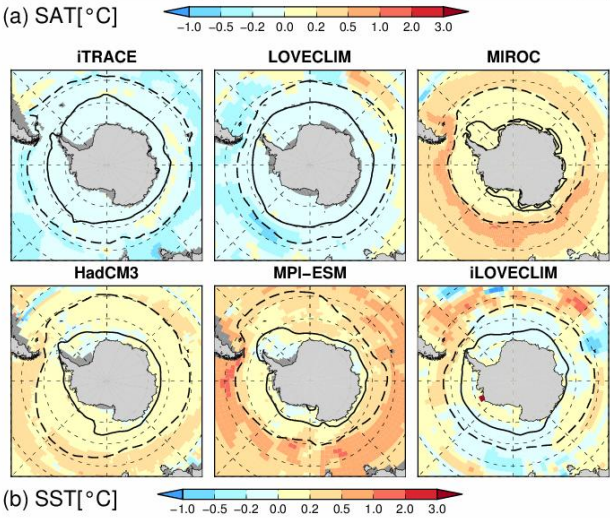
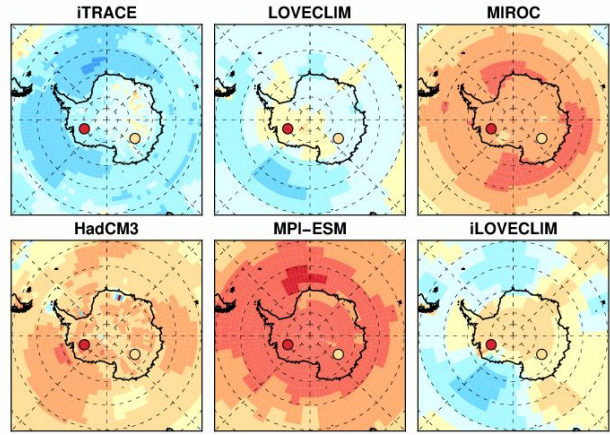


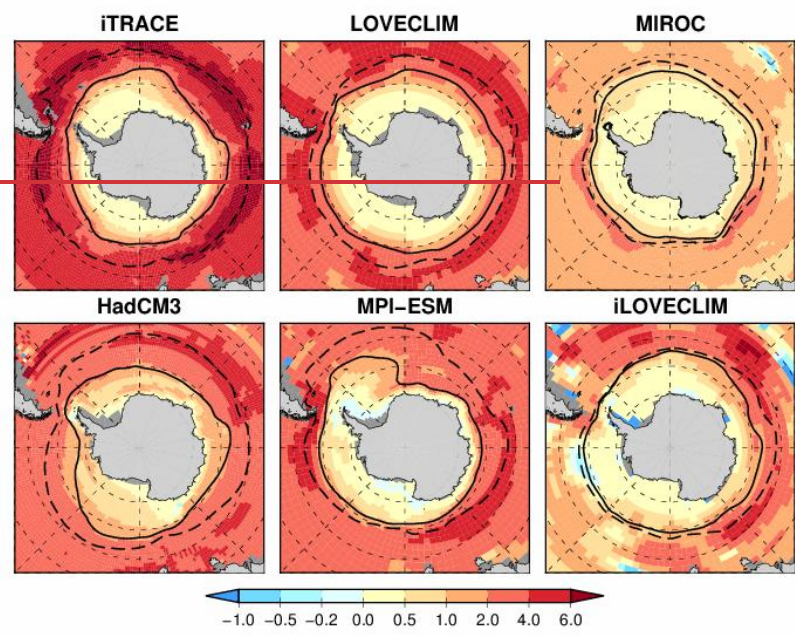
Figure 3: Time series of (a) atmospheric CO₂ (Bereiter et al., 2015) and (b) simulated AMOC, (c–d) SAT at WDC and EDC, (e) Southern Ocean SST (zonal mean SST in the latitude band 55–40°S), (f) Southern Ocean sea ice area in the transient simulations. The SAT, SST and sea ice area indicate changes since the LGM. The grey lines in (c–d) represent reconstructions from Buizert et al., (2013), and the black line in (d) represents reconstructions from Parrenin et al., (2013). The black lines and grey shades in (e) indicate the Southern Ocean SST stack and its standard error, respectively, as derived by Anderson et al., (2020).

652 The vertical grey shading indicates HS1 (18–14.7 ka) and the YD (12.8–11.7 ka), respectively, and the
653 period in between corresponds to the BA (14.7–12.8 ka).

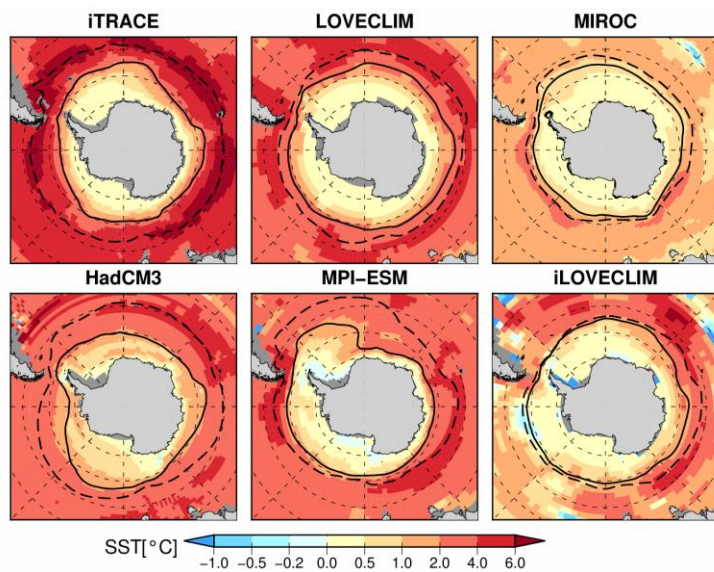
書式を変更: フォント: (日) + 本文のフォント - 日本語 (MS 明朝)



656 **Figure 4:** (a) SAT and (b) SST anomalies at 18 ka compared to the LGM. The coloured circles in (a)
657 represent 18 ka-LGM SAT change based on ice core data (Parrenin et al., 2013), and the bold and dashed
658 lines in (b) represent LGM austral summer and winter sea ice extent (85 and 15% annual-mean sea ice
659 concentration), respectively.

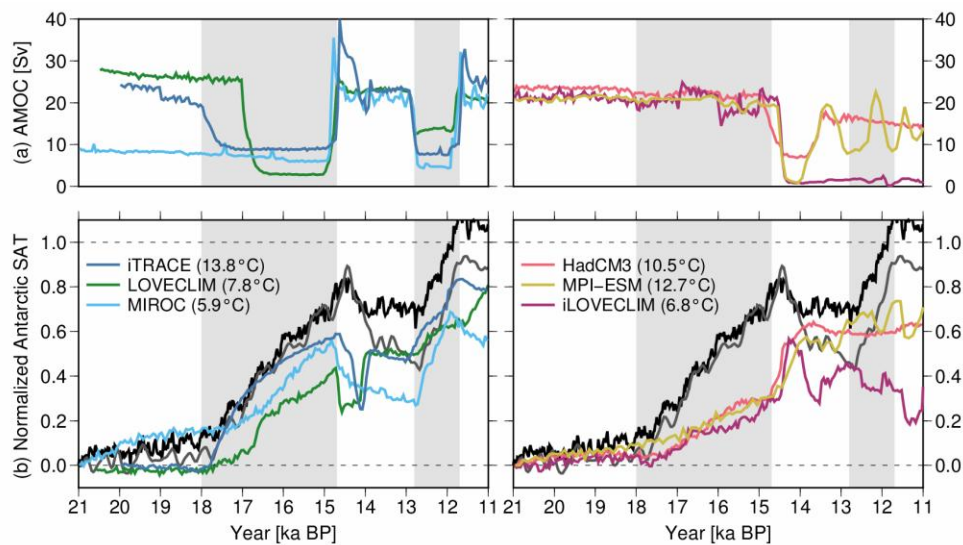
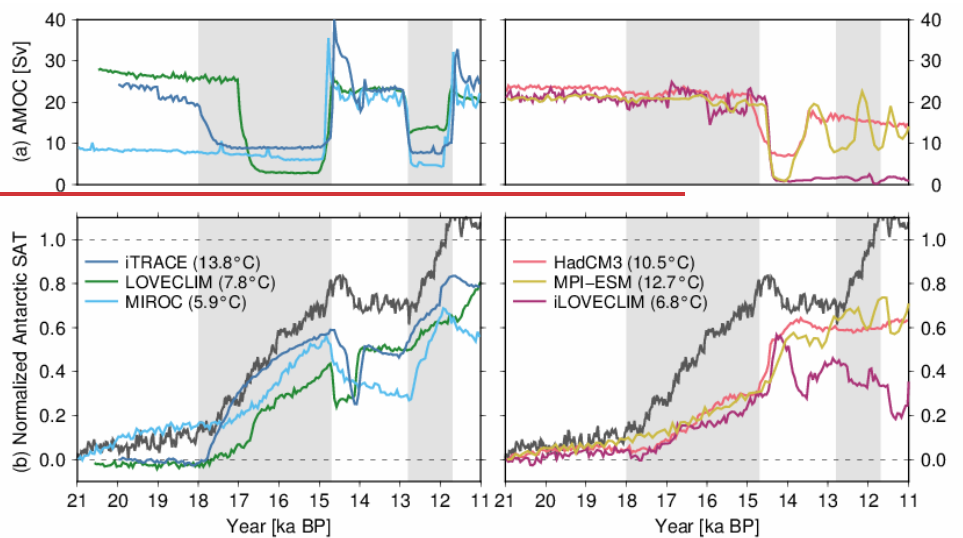


660



書式を変更: フォント: (日) + 本文のフォント - 日本語 (MS 明朝), (言語 1) 日本語

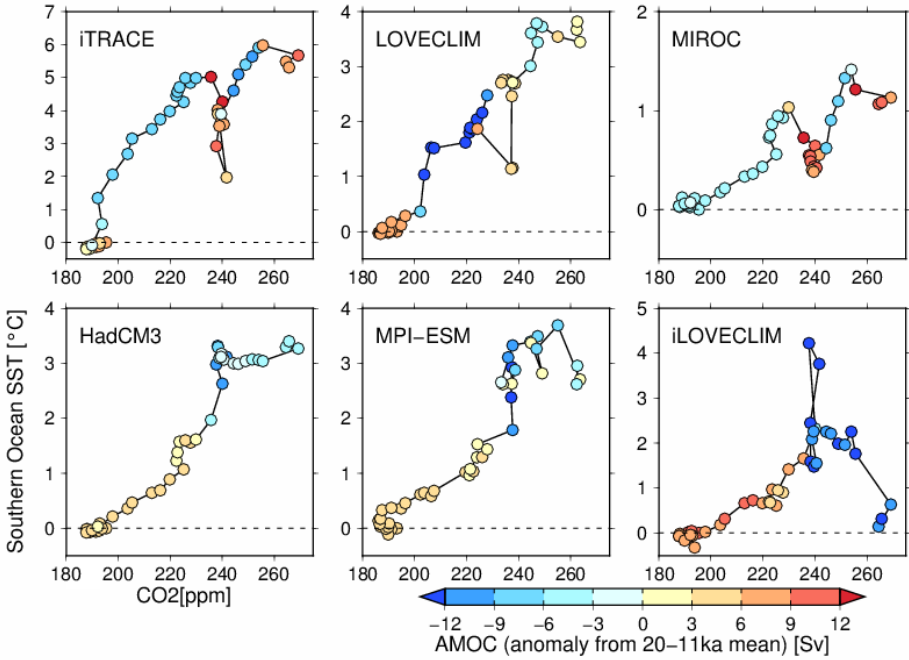
Figure 5: SST anomalies at 11 ka compared to the LGM. The bold and dashed lines indicate LGM and 11 ka sea ice extent (15% sea ice concentration), respectively.



666
667
668
669
670
671

Figure 6: AMOC and normalised Antarctic SAT, with respect to the difference between PI and LGM. The actual PI and LGM differences are indicated in parentheses. The left panels show three simulations with weak AMOC during HS1, and the right show strong AMOC during HS1, respectively. The grey and black lines in (b) is normalised Antarctic SAT from EDC based on Parrenin et al., (2013) and Buizert et al., (2021), respectively. The vertical grey shading indicates HS1 (18–14.7 ka) and the YD (12.8–11.7 ka), respectively, and the period in between corresponds to the BA (14.7–12.8 ka).

書式を変更: フォント: (日) + 本文のフォント - 日本語 (MS 明朝), (言語 1) 日本語



672
673
674
675
676
677

Figure 7: Relationship between Southern Ocean SST (vertical axis, change since LGM), CO₂ (horizontal axis) and AMOC strength anomaly from the mean strength between 20–11 ka (colours). The trajectory of the deglacial CO₂ forcing (CO₂), simulated SST changes and AMOC are plotted with circles at 200-year intervals. Note that the vertical axes are different between models to represent the total deglacial warming.

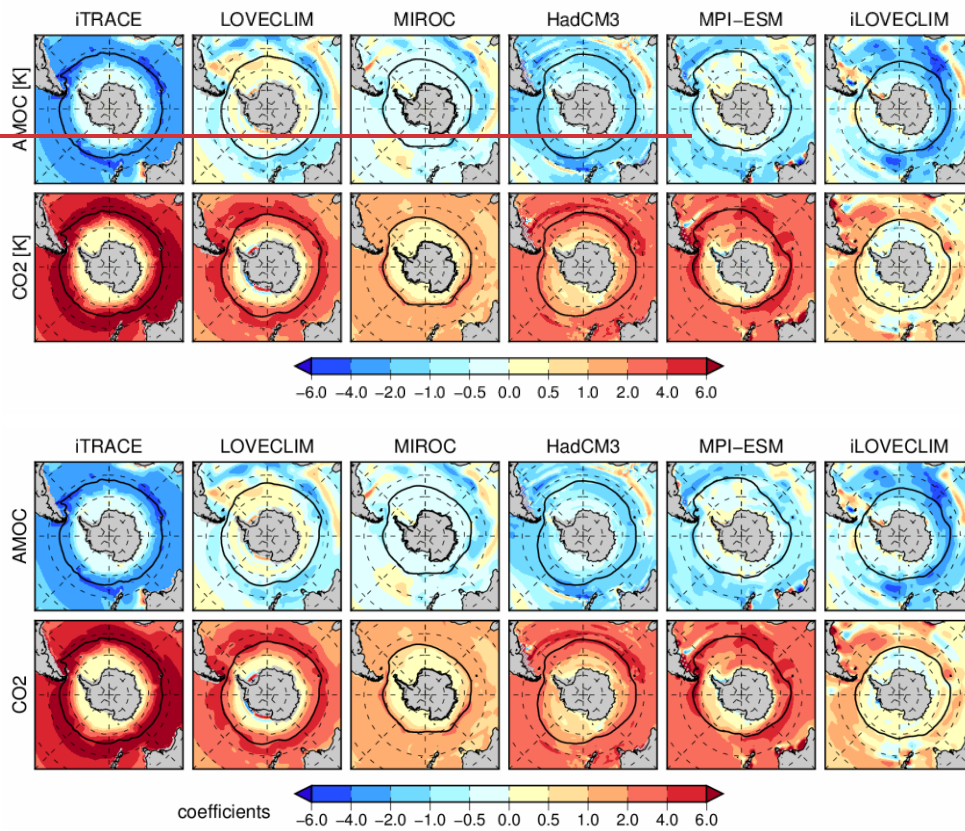


Figure 8: Results of the MLR model for 2-D SST maps. Top and bottom panels indicate \pm AMOC coefficients [K/normalised AMOC] and \pm CO₂ coefficients [K/83 ppm]. The black lines represent LGM winter sea ice edges.

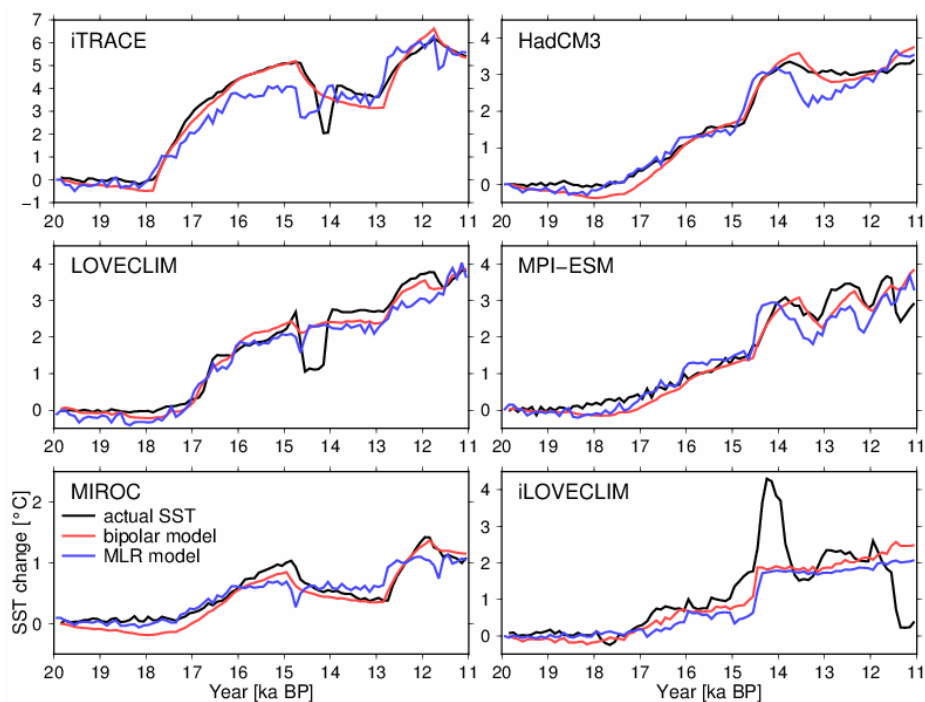


Figure 9: Results of the MLR model and bipolar seesaw model for Southern Ocean SST. The black lines represent the actual SST change (anomaly from 20 ka). The blue and red lines represent the results of MLR and bipolar seesaw models, respectively.

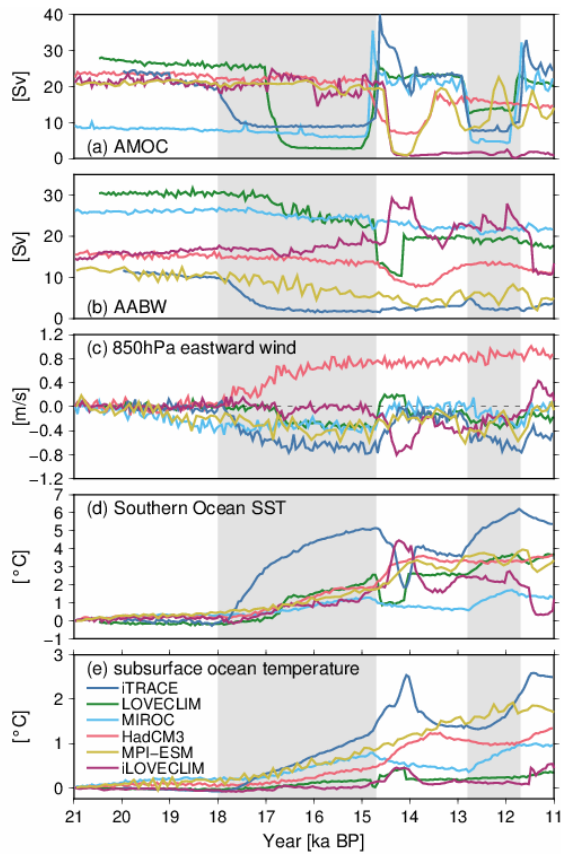
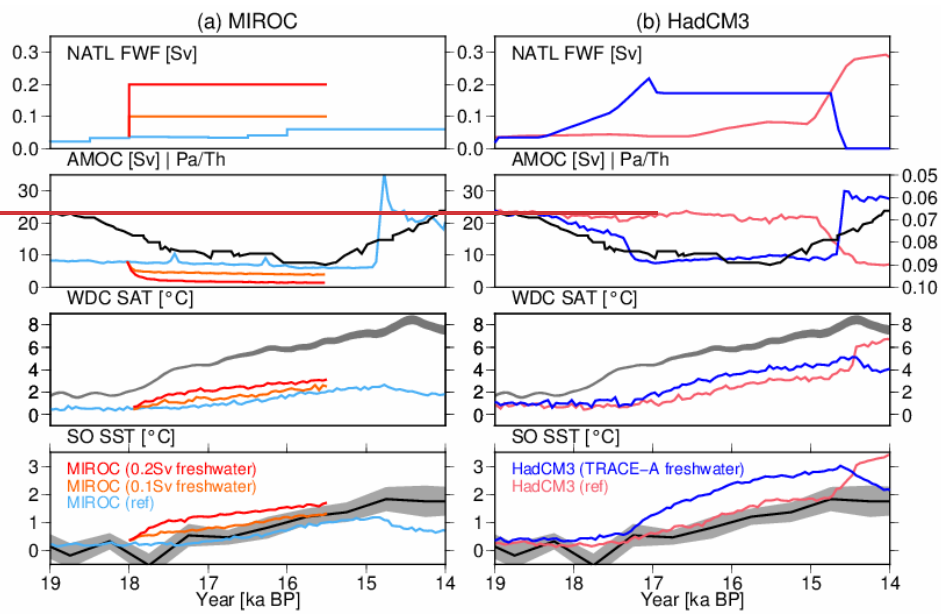


Figure 10: Time series of simulated (a) AMOC, (b) AABW, (c) 850_hPa eastward winds over the Southern Ocean (65–40°S), (d) Southern Ocean SST, and (e) subsurface ocean temperature south of 60°S (at depths 400–666m). The vertical grey shading indicates HS1 (18–14.7 ka) and the YD (12.8–11.7 ka), respectively, and the period in between corresponds to the BA (14.7–12.8 ka).



694

695

696

697

698

699

700

701

702

703

704

705

706

707

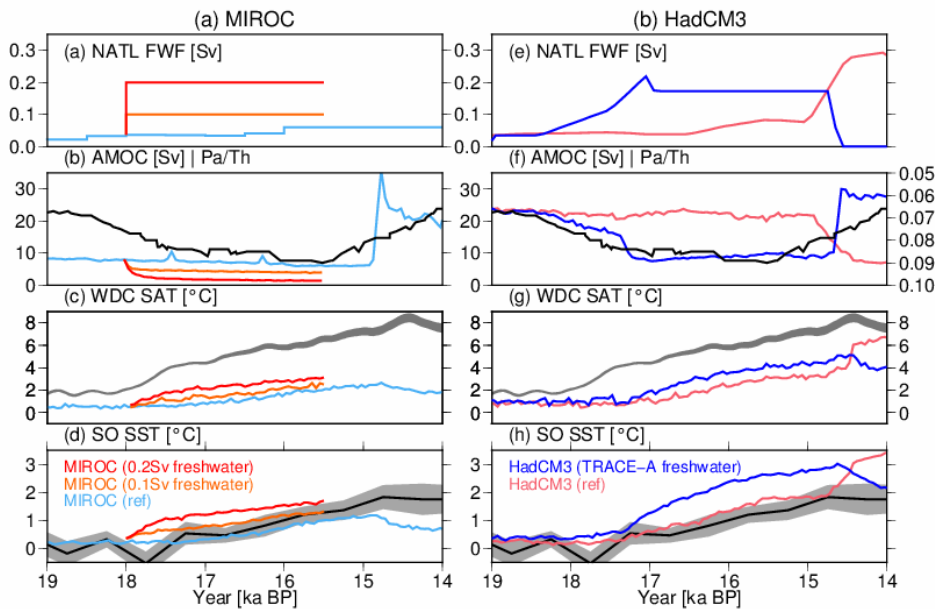


Figure 11: Results from transient deglaciation experiments performed with (a) MIROC and (b) HadCM3. The black lines in each panel represent the same proxy data as in Figure 3 (Parrenin et al., 2013; Buizert et al., 2021; Anderson et al., 2020). In two MIROC sensitivity experiments, a larger amount of freshwater flux (0.1 or 0.2 Sv) is added into the North Atlantic (50–70°N) during 18–15.5 ka compared to the standard MIROC experiment (light blue lines). In the TRACE-A HadCM3 sensitivity experiment (blue lines), a larger freshwater flux is added in the North Atlantic following the Trace-21ka simulation (Liu et al., 2009), while the pink lines in (b) represent the HadCM3 simulation used in Snoll et al. (2022).

References

1. Abe-Ouchi, A., Saito, F., Kawamura, K., Raymo, M. E., Okuno, J., Takahashi, K., and Blatter, H.: Insolation-driven 100,000-year glacial cycles and hysteresis of ice-sheet volume. *Nature* 500, 190–193, doi: 10.1038/nature12374, 2013.

書式を変更: フォント: (日) Times New Roman

708 [+2. Abe-Ouchi, A., Saito, F., Kageyama, M., Braconnot, P., Harrison, S. P., Lambeck, K., Otto-Bliesner,](#)
709 [B. L., Peltier, W. R., Tarasov, L., Peterschmitt, J.-Y., and Takahashi, K.: Ice-sheet configuration in](#)
710 [the CMIP5/PMIP3 Last Glacial Maximum experiments, *Geosci. Model Dev.*, **8**, 3621?3637,](#)
711 [doi:10.5194/gmd-8-3621-2015, 2015.](#)

712 [2-3. Anderson, B. E., & Burckle, L. H.: Rise in Atmospheric CO₂. *Science*, **323** \(March\), 1443–1448,](#)
713 [2009](#)

714 [3-4. Anderson, H. J., Pedro, J. B., Bostock, H. C., Chase, Z., and Noble, T. L.: Compiled Southern Ocean](#)
715 [sea surface temperatures correlate with Antarctic Isotope Maxima, *Quaternary Science Reviews*, **255**,](#)
716 [106821, <https://doi.org/10.1016/j.quascirev.2021.106821>, 2021.](#)

717 [4-5. Anderson, Harris J; Pedro, Joel B; Bostock, Helen C; Chase, Zanna; Noble, Taryn L \(2020\): Southern](#)
718 [Ocean Sea Surface Temperature Anomaly Stacks \[dataset\]. PANGAEA,](#)
719 [https://doi.org/10.1594/PANGAEA.912158](#)

720 [5-6. Annan, J. D., Hargreaves, J. C., and Mauritsen, T.: A new global surface temperature reconstruction](#)
721 [for the Last Glacial Maximum, *Clim. Past*, **18**, 1883–1896, <https://doi.org/10.5194/cp-18-1883-2022>,](#)
722 [2022.](#)

723 [6-7. Bentley, M. J., Ocofaigh, C., Anderson, J. B., Conway, H., Davies, B., Graham, A. G. C., Hillenbrand,](#)
724 [C. D., Hodgson, D. A., Jamieson, S. S. R., Larter, R. D., Mackintosh, A., Smith, J. A., Verleyen, E.,](#)
725 [Ackert, R. P., Bart, P. J., Berg, S., Brunstein, D., Canals, M., Colhoun, E. A., Crosta, X., Dickens,](#)
726 [W. A., Domack, E., Dowdeswell, J. A., Dunbar, R., Ehrmann, W., Evans, J., Favier, V., Fink, D.,](#)
727 [Fogwill, C. J., Glasser, N. F., Gohl, K., Golledge, N. R., Goodwin, I., Gore, D. B., Greenwood, S. L.,](#)
728 [Hall, B. L., Hall, K., Hedding, D. W., Hein, A. S., Hocking, E. P., Jakobsson, M., Johnson, J. S.,](#)
729 [Jomelli, V., Jones, R. S., Klages, J. P., Kristoffersen, Y., Kuhn, G., Leventer, A., Licht, K., Lilly, K.,](#)
730 [Lindow, J., Livingstone, S. J., Massé, G., McGlone, M. S., McKay, R. M., Melles, M., Miura, H.,](#)
731 [Mulaney, R., Nel, W., Nitsche, F. O., O'Brien, P. E., Post, A. L., Roberts, S. J., Saunders, K. M.,](#)
732 [Selkirk, P. M., Simms, A. R., Spiegel, C., Stollendorf, T. D., Sugden, D. E., van der Putten, N., van](#)
733 [Ommen, T., Verfaillie, D., Vyverman, W., Wagner, B., White, D. A., Witus, A. E., and Zwartz, D.:](#)
734 [A community-based geological reconstruction of Antarctic Ice Sheet deglaciation since the Last](#)

735 Glacial Maximum, *Quaternary Sci. Rev.*, 100, 1–9, <https://doi.org/10.1016/j.quascirev.2014.06.025>,
736 2014.

737 ~~7-8.~~ Berger, A.: Long-Term Variations of Daily Insolation and Quaternary Climatic Changes, *J. Atmos.*
738 *Sci.*, 35, 2362–2367, doi:10.1175/1520-0469(1978)035<2362:LTVODI>2.0.CO;2, 1978.

739 ~~8-9.~~ Bereiter, B., Eggleston, S., Schmitt, J., Nehrbass-Ahles, C., Stocker, T. F., Fischer, H., Kipfstuhl, S.,
740 and Chappellaz, J.: Revision of the EPICA Dome C CO₂ record from 800 to 600 kyr before present,
741 *Geophys. Res. Lett.*, 42, 542–549, 10.1002/2014GL061957, 2015.

742 ~~9-10.~~ Bereiter, B., Shackleton, S., Baggenstos, D., Kawamura, K., and Severinghaus, J.: Mean global
743 ocean temperatures during the last glacial transition. *Nature*, 553(7686), 39–44.
744 <https://doi.org/10.1038/nature25152>, 2018.

745 ~~10-11.~~ Bethke, I., Li, C., and Nisancioglu, K. H.: Can we use ice sheet reconstructions to constrain
746 meltwater for deglacial simulations? *Paleoceanography*, 27 (November 2011), 1–17.
747 doi:10.1029/2011PA002258, 2012

748 ~~11-12.~~ Böhm, E., Lippold, J., Gutjahr, M., Frank, M., Blaser, P., Antz, B., Fohlmeister, J., Frank, N.,
749 Andersen, M. B. and Deininger, M.: Strong and deep Atlantic meridional overturning circulation
750 during the last glacial cycle. *Nature*, 517(7534), 73–76. <https://doi.org/10.1038/nature14059>, 2015.

751 ~~12-13.~~ Bouttes, N., Roche, D. M., and Paillard, D.: Systematic study of the impact of fresh water fluxes
752 on the glacial carbon cycle, *Clim. Past*, 8, 589–607, <https://doi.org/10.5194/cp-8-589-2012>, 2012.

753 ~~13-14.~~ Bouttes, N., Lhardy, F., Quiquet, A., Paillard, D., Goosse, H., and Roche, D. M.: Deglacial climate
754 changes as forced by different ice sheet reconstructions, *Clim. Past*, 19, 1027–1042,
755 <https://doi.org/10.5194/cp-19-1027-2023>, 2023.

756 ~~14-15.~~ Buizert, C., Gkinis, V., Severinghaus, J. P., He, F., Lecavalier, B. S., Kindler, P., Leuenberger,
757 M., Carlson, A. E., Vinther, B., Masson-Delmotte, V., White, J. W. C., Liu, Z., Otto-Bliesner, B.,
758 and Brook, E. J.: Greenland temperature response to climate forcing during the last deglaciation,
759 *Science*, 345, 1177–1180, 10.1126/science.1254961, 2014.

760 ~~15-16.~~ Buizert, C., Fudge, T. J., Roberts, W. H., Steig, E. J., Sherriff-Tadano, S., Ritz, C., Lefebvre, E.,
761 Edwards, J., Kawamura, K., Oyabu, I., Motoyama, H. Kahle, E. C., Jones, T. R., Abe-ouchi, A.,
762 Obase, T., Martin, C., Corr, H., Severinghaus, J. P., Beaudette, R. Epifanio, J. A., Brook, E. J., Martin,

763 K., Aoki, S., Nakazawa, T., Sowers, T. A., Alley, R. B., Ahn, J., Sigl, M., Severi, M., Dunbar, N. W.,
764 Svensson, A., Fegyveresi, J. M., He, C., Liu, Z., Zhu, J., Otto-bliesner, B. L., Lipenkov, V. Y.,
765 Kageyama, M., and Schwander, J.: Antarctic surface temperature and elevation during the Last
766 Glacial Maximum, *Science* 372(6546), 1097-1101, doi: 10.1126/science.abd2897, 2021

767 ~~16-17.~~ Burke, A. and Robinson, L. F.: The Southern Ocean's Role in Carbon Exchange During the Last
768 Deglaciation, *Science*, 135, 6068, 557-561. <https://doi.org/10.1126/science.1208163>, 2011

769 ~~17-18.~~ Capron, E., Landais, A., Chappellaz, J., Schilt, A., Buiron, D., Dahl-Jensen, D., Johnsen, S. J.,
770 Jouzel, J., Lemieux-Dudon, B., Loulergue, L., Leuenberger, M., Masson-Delmotte, V., Meyer, H.,
771 Oerter, H., and Stenni, B.: Millennial and sub-millennial scale climatic variations recorded in polar
772 ice cores over the last glacial period, *Clim. Past*, 6, 345–365, <https://doi.org/10.5194/cp-6-345-2010>,
773 2010.

774 ~~18-19.~~ Chan, W.-L. and Abe-Ouchi, A.: Pliocene Model Intercomparison Project (PlioMIP2) simulations
775 using the Model for Interdisciplinary Research on Climate (MIROC4m), *Clim. Past*, 16, 1523–1545,
776 <https://doi.org/10.5194/cp-16-1523-2020>, 2020.

777 ~~19-20.~~ Clark, P. U., He, F., Golledge, N. R., Mitrovica, J. X., Dutton, A., Hoffman, J. S., and Dendy,
778 S.: Oceanic forcing of penultimate deglacial and last interglacial sea-level rise. *Nature*, 577(7792),
779 660–664. <https://doi.org/10.1038/s41586-020-1931-7>, 2020

780 ~~20-21.~~ Condon, A., & Winsor, P.: Meltwater routing and the Younger Dryas. *Proceedings of the*
781 *National Academy of Sciences*, 109(49), 19928–19933, <https://doi.org/10.1073/pnas.1207381109>,
782 2012

783 ~~21-22.~~ Crosta, X., Kohfeld, K. E., Bostock, H. C., Chadwick, M., Du Vivier, A., Esper, O., Etourneau,
784 J., Jones, J., Leventer, A., Müller, J., Rhodes, R. H., Allen, C. S., Ghadi, P., Lamping, N., Lange, C.
785 B., Lawler, K.-A., Lund, D., Marzocchi, A., Meissner, K. J., Menviel, L., Nair, A., Patterson, M.,
786 Pike, J., Prebble, J. G., Riesselman, C., Sadatzki, H., Sime, L. C., Shukla, S. K., Thöle, L., Vorrath,
787 M.-E., Xiao, W., and Yang, J.: Antarctic sea ice over the past 130 000 years – Part 1: a review of
788 what proxy records tell us, *Clim. Past*, 18, 1729–1756, <https://doi.org/10.5194/cp-18-1729-2022>,
789 2022.

790 [22-23.](#) Dansgaard, W., Johnsen, S. J., Clausen, H. B., Dahl-Jensen, D., Gundestrup, N. S., Hammer, C.
791 U., Hvidberg, C. S., Steffensen, J. P., Sveinbjörnsdottir, A. E., Jouzel, J., and Bond, G.: Evidence for
792 general instability of past climate from a 250-kyr ice-core record, *Nature*, 364, 218–220,
793 <https://doi.org/10.1038/364218a0>, 1993

794 [24.](#) Deschamps, P., Durand, N., Bard, E., Hamelin, B., Camoin, G., Thomas, A. L., Henderson, G. M.,
795 Okuno, J., and Yokoyama, Y.: Ice-sheet collapse and sea-level rise at the Bølling warming 14,600
796 years ago, *Nature*, 28, 559–564, <https://doi.org/10.1038/nature10902>, 2012. ▲

797 [23-25.](#) Ferrari, R., Jansen, M. F., Adkins, J. F., Burke, A., Stewart, A. L., and Thompson, A. F.: Antarctic
798 sea ice control on ocean circulation in present and glacial climates, *P. Natl. Acad. Sci. USA*, 111,
799 [8753–8758, 10.1073/pnas.1323922111, 2014.](#)

800 [24-26.](#) Golledge, N., Menviel, L., Carter, L., Fogwill, C. J., England, M. H., Cortese, G., and Levy, R.
801 H.: Antarctic contribution to meltwater pulse 1A from reduced Southern Ocean overturning. *Nat*
802 *Commun* 5, 5107, <https://doi.org/10.1038/ncomms6107>, 2014.

803 [25-27.](#) Gomez, N., Weber, M. E., Clark, P. U., Mitrovica, J. X. and Han, H. K.: Antarctic ice dynamics
804 amplified by Northern Hemisphere sea-level forcing, *Nature*, 587(7835), 600–604,
805 [doi:10.1038/s41586-020-2916-2](https://doi.org/10.1038/s41586-020-2916-2), 2020

806 [26-28.](#) Goosse, H., Brovkin, V., Fichefet, T., Haarsma, R., Huybrechts, P., Jongma, J., Mouchet, A.,
807 Selten, F., Barriat, P.-Y., Campin, J.-M., Deleersnijder, E., Driesschaert, E., Goelzer, H., Janssens, I.,
808 Loutre, M.-F., Morales Maqueda, M. A., Opsteegh, T., Mathieu, P.-P., Munhoven, G., Pettersson, E.
809 J., Renssen, H., Roche, D. M., Schaeffer, M., Tartinvill, B., Timmermann, A., and Weber, S. L.:
810 Description of the Earth system model of intermediate complexity LOVECLIM version 1.2, *Geosci.*
811 *Model Dev.*, 3, 603–633, <https://doi.org/10.5194/gmd-3-603-2010>, 2010.

812 [27-29.](#) Gottschalk, J., Battaglia, G., Fischer, H., Frölicher, T. L., Jaccard, S. L., Jeltsch-Thömmes, A.,
813 Joos, F., Köhler, P., Meissner, K. J., Menviel, L., Nehrbass-Ahles, C., Schmitt, J., Schmittner, A.,
814 Skinner, L. C., and Stocker, T. F.: Mechanisms of millennial-scale atmospheric CO₂ change in
815 numerical model simulations, *Quaternary Sci. Rev.*, 220, 30–74,
816 <https://doi.org/10.1016/j.quascirev.2019.05.013>, 2019.

書式を変更: フォント: (日) Times New Roman

817 ~~28-30.~~ Gray, W. R., de Lavergne, C., Willis, R. C. J., Menviel, L., Spence, P., Holzer, M., Kageyama, M.
818 and Michel, E.: Poleward Shift in the Southern Hemisphere Westerly Winds Synchronous With the
819 Deglacial Rise in CO₂, *Paleoceanography and Paleoclimatology*, 38, 7,
820 <https://doi.org/10.1029/2023PA004666>, 2023

821 ~~29-31.~~ Green, R. A., Menviel, L., Meissner, K. J., Crosta, X., Chandan, D., Lohmann, G., Peltier, W. R.,
822 Shi, X., and Zhu, J.: Evaluating seasonal sea-ice cover over the Southern Ocean at the Last Glacial
823 Maximum, *Clim. Past*, 18, 845–862, <https://doi.org/10.5194/cp-18-845-2022>, 2022.

824 ~~30-32.~~ Gregoire, L. J., Payne, A. J., and Valdes, P. J.: Deglacial rapid sea level rises caused by ice-sheet
825 saddle collapses, *Nature*, 487, 219–222, [10.1038/nature11257](https://doi.org/10.1038/nature11257), 2012.

826 ~~31-33.~~ He, F., Shakun, J. D., Clark, P. U., Carlson, A. E., Liu, Z., Otto-Bliesner, B. L., and Kutzbach, J.
827 E.: Northern Hemisphere forcing of Southern Hemisphere climate during the last deglaciation, *Nature*,
828 494, 81-85, <https://doi.org/10.1038/nature11822>, 2013.

829 ~~32-34.~~ He, C., Zhengyu Liu, and Aixue Hu.: The transient response of atmospheric and oceanic heat
830 transports to anthropogenic warming. *Nature Climate Change*, 1, [doi:10.1038/s41558-018-0387-3](https://doi.org/10.1038/s41558-018-0387-3),
831 2019.

832 ~~33-35.~~ He, C., Liu, Z., Zhu, J., Zhang, J., Gu, S., Otto-Bliesner, B. L., Brady, E., Zhu, C., Jin, Y. and Sun,
833 J.: North Atlantic subsurface temperature response controlled by effective freshwater input in
834 “Heinrich” events, *Earth and Planetary Science Letters*, 539, 116247,
835 <https://doi.org/10.1016/j.epsl.2020.116247>, 2020.

836 ~~34-36.~~ He, C., Liu, Z., Otto-Bliesner, B. L., Brady, E. C., Zhu, C., Tomas, R., Bao, Y.: Hydroclimate
837 footprint of pan-Asian monsoon water isotope during the last deglaciation. *Science Advances*, 7(4),
838 1–12. <https://doi.org/10.1126/sciadv.abe2611>, 2021.

839 ~~35-37.~~ Hunter, S. J., Haywood, A. M., Dolan, A. M., and Tindall, J. C.: The HadCM3 contribution to
840 PlioMIP phase 2, *Clim. Past*, 15, 1691–1713, <https://doi.org/10.5194/cp-15-1691-2019>, 2019.

841 ~~36-38.~~ Ivanovic, R. F., Gregoire, L. J., Kageyama, M., Roche, D. M., Valdes, P. J., Burke, A., Drummond,
842 R., Peltier, W. R., and Tarasov, L.: Transient climate simulations of the deglaciation 21–9 thousand
843 years before present (version 1) – PMIP4 Core experiment design and boundary conditions, *Geosci.*
844 *Model Dev.*, 9, 2563–2587, <https://doi.org/10.5194/gmd-9-2563-2016>, 2016.

845 ~~37-39.~~ Ivanovic, R. F., Gregoire, L. J., Burke, A., Wickert, A. D., and Valdes, P. J.: Acceleration of
846 Northern Ice Sheet Melt Induces AMOC Slowdown and Northern Cooling in Simulations of the Early
847 Last Deglaciation, *Paleoceanography and Paleoclimatology*, 807–824. doi:10.1029/2017PA003308,
848 2018

849 ~~38-40.~~ Jouzel, J., Masson-Delmotte, V., Cattani, O., Dreyfus, G., Falourd, S., Hoffmann, G., Minster, B.,
850 Nouet, J., Barnola, J. M., Chappellaz, J., Fischer, H., Gallet, J. C., Johnsen, S., Leuen-berger, M.,
851 Loulergue, L., Luethi, D., Oerter, H., Parrenin, F., Raisbeck, G., Raynaud, D., Schilt, A., Schwander,
852 J., Selmo, E., Souchez, R., Spahni, R., Stauffer, B., Steffensen, J. P., Stenni, B., Stocker, T. F., Tison,
853 J. L., Werner, M., and Wolff, E. W.: Orbital and Millennial Antarctic Climate Variability over the
854 Past 800,000 Years, *Science*, 317, 793-796, <https://doi.org/10.1126/science.1141038>, 2007.

855 ~~39-41.~~ Kageyama, M., Merkel, U., Otto-Bliesner, B., Prange, M., Abe-Ouchi, A., Lohmann, G., Ohgaito,
856 R., Roche, D. M., Singarayer, J., Swingedouw, D., and X Zhang: Climatic impacts of fresh water
857 hosing under Last Glacial Maximum conditions: a multi-model study, *Clim. Past*, 9, 935–953,
858 <https://doi.org/10.5194/cp-9-935-2013>, 2013.

859 ~~40-42.~~ Kageyama, M., Braconnot, P., Harrison, S. P., Haywood, A. M., Jungclaus, J. H., Otto-Bliesner,
860 B. L., Peterschmitt, J.-Y., Abe-Ouchi, A., Albani, S., Bartlein, P. J., Brierley, C., Crucifix, M., Dolan,
861 A., Fernandez-Donado, L., Fischer, H., Hopcroft, P. O., Ivanovic, R. F., Lambert, F., Lunt, D. J.,
862 Mahowald, N. M., Peltier, W. R., Phipps, S. J., Roche, D. M., Schmidt, G. A., Tarasov, L., Valdes,
863 P. J., Zhang, Q., and Zhou, T.: The PMIP4 contribution to CMIP6 – Part 1: Overview and over-
864 arching analysis plan, *Geosci. Model Dev.*, 11, 1033–1057, [https://doi.org/10.5194/gmd-11-1033-](https://doi.org/10.5194/gmd-11-1033-2018)
865 2018, 2018.

866 ~~41-43.~~ Kageyama, M., Harrison, S. P., Kapsch, M.-L., Lofverstrom, M., Lora, J. M., Mikolajewicz, U.,
867 Sherriff-Tadano, S., Vadsaria, T., Abe-Ouchi, A., Bouttes, N., Chandan, D., Gregoire, L. J., Ivanovic,
868 R. F., Izumi, K., LeGrande, A. N., Lhardy, F., Lohmann, G., Morozova, P. A., Ohgaito, R., Paul, A.,
869 Peltier, W. R., Poulsen, C. J., Quiquet, A., Roche, D. M., Shi, X., Tierney, J. E., Valdes, P. J., Volodin,
870 E., and Zhu, J.: The PMIP4 Last Glacial Maximum experiments: preliminary results and comparison
871 with the PMIP3 simulations, *Clim. Past*, 17, 1065–1089, <https://doi.org/10.5194/cp-17-1065-2021>,
872 2021.

873 ~~42-44.~~ Kapsch, M.-L., Mikolajewicz, U., Ziemen, F. and Schannwell, C.: Ocean response in transient
874 simulations of the last deglaciation dominated by underlying ice-sheet reconstruction and method of
875 meltwater distribution, *Geophysical Research Letters*, 49, e2021GL096767,
876 <https://doi.org/10.1029/2021GL096767>, 2022.

877 ~~43-45.~~ Kobayashi, H., Oka, A., Yamamoto, A., and Abe-Ouchi, A.: Glacial carbon cycle changes by
878 Southern Ocean processes with sedimentary amplification. *Science Advances*, 7(35), doi:
879 10.1126/sciadv.abg7723, 2021.

880 ~~46.~~ Kobayashi, H., Oka, A., Obase, T., and Abe-Ouchi, A.: Assessing transient changes in the ocean
881 carbon cycle during the last deglaciation through carbon isotope modeling, *Clim. Past*, 20, 769–787,
882 <https://doi.org/10.5194/cp-20-769-2024>, 2024.

883 ~~44.~~

884 ~~45-47.~~ Kuniyoshi, Y., Abe-Ouchi, A., Sherriff-Tadano, S., Chan, W.-L., and Saito, F.: Effect of Climatic
885 Precession on Dansgaard-Oeschger-Like Oscillations. *Geophysical Research Letters*, 49(6),
886 e2021GL095695. <https://doi.org/10.1029/2021GL095695>, 2022.

887 ~~46-48.~~ Lambeck, K., Rouby, H., Purcell, A., Sun, Y., and Sambridge, M.: Sea level and global ice
888 volumes from the Last Glacial Maximum to the Holocene, *P. Natl. Acad. Sci.*, 111, 15296–15303,
889 10.1073/pnas.1411762111, 2014.

890 ~~47-49.~~ Lhardy, F., Bouttes, N., Roche, D. M., Crosta, X., Waelbroeck, C., and Paillard, D.: Impact of
891 Southern Ocean surface conditions on deep ocean circulation during the LGM: a model analysis,
892 *Clim. Past*, 17, 1139–1159, <https://doi.org/10.5194/cp-17-1139-2021>, 2021.

893 ~~48-50.~~ Lisiecki, L. E. and Raymo, M. E.: A Pliocene-Pleistocene stack of 57 globally distributed benthic
894 $\delta^{18}\text{O}$ records, *Paleoceanography*, 20, PA1003, doi:10.1029/2004PA001071, 2005

895 ~~49-51.~~ Liu, Z., Otto-Bliesner, B. L., He, F., Brady, E. C., Tomas, R., Clark, P. U., Carlson, A. E., Lynch-
896 Stieglitz, J., Curry, W., Brook, E., Erickson, D., Jacob, R., Kutzbach, J., and Cheng, J.: Transient
897 Simulation of Last Deglaciation with a New Mechanism for Bølling-Allerød Warming, *Science*, 325,
898 310–314, doi:10.1126/science.1171041, 2009

899 ~~50-52.~~ Liu, Z., Bao, Y., Thompson, L. G., Mosley-Thompson, E., Tabor, C., Zhang, G. J., Yan, M.,
900 Lofverstrom, M., Montanez, I., and Oster, J.: Tropical mountain ice core $\delta^{18}\text{O}$: A Goldilocks

書式を変更: フォント: (日) Times New Roman

901 indicator for global temperature change, *Science Advances*, 9, 45,
 902 <https://doi.org/10.1126/sciadv.adi6725>, 2023

903 ~~51-53.~~ Love, R., Andres, H. J., Condron, A., and Tarasov, L.: Freshwater routing in eddy-permitting
 904 simulations of the last deglacial: the impact of realistic freshwater discharge, *Clim. Past*, 17, 2327–
 905 2341, <https://doi.org/10.5194/cp-17-2327-2021>, 2021.

906 ~~52-54.~~ Lowry, D. P., Golledge, N. R., Menviel, L., and Bertler, N. A. N.: Deglacial evolution of regional
 907 Antarctic climate and Southern Ocean conditions in transient climate simulations. 189–215, 2018.

908 ~~53-55.~~ Lynch-Stieglitz, J., Adkins, J. F., Curry, W. B., Dokken, T., Hall, I. R., Herguera, J. C. and Zahn,
 909 R.: Atlantic meridional overturning circulation during the Last Glacial Maximum. *Science*,
 910 316(5821), 66–69. <https://doi.org/10.1126/science.1137127>, 2007

911 ~~54-56.~~ MacDougall, A. H., Frölicher, T. L., Jones, C. D., Rogelj, J., Matthews, H. D., Zickfeld, K., Arora,
 912 V. K., Barrett, N. J., Brovkin, V., Burger, F. A., Eby, M., Eliseev, A. V., Hajima, T., Holden, P. B.,
 913 Jeltsch-Thömmes, A., Koven, C., Mengis, N., Menviel, L., Michou, M., Mokhov, I. I., Oka, A.,
 914 Schwinger, J., Séférian, R., Shaffer, G., Sokolov, A., Tachiiri, K., Tjiputra, J., Wiltshire, A., and
 915 Ziehn, T.: Is there warming in the pipeline? A multi-model analysis of the Zero Emissions
 916 Commitment from CO₂, *Biogeosciences*, 17, 2987–3016, <https://doi.org/10.5194/bg-17-2987-2020>,
 917 2020.

918 ~~55-57.~~ Marcott, S. A., Bauska, T. K., Buizert, C., Steig, E. J., Rosen, J. L., Cuffey, K. M., Fudge, T. J.,
 919 Severinghaus, J. P., Kalk, M. L., McConnell, J. R., Sowers, T., Taylor, K. C. White, J. W. C. and
 920 Brook, E. J.: Centennial-scale changes in the global carbon cycle during the last deglaciation. *Nature*,
 921 514(7524), 616–619. <https://doi.org/10.1038/nature13799>, 2014

922 ~~56-58.~~ Margari, V., Skinner, L. C., Menviel, L., Capron, E., Rhodes, R. H., Martrat, B., and Grimalt, J.
 923 O.: Fast and slow components of interstadial warming in the North Atlantic during the last glacial.
 924 *Communications Earth & Environment*, 1–9. <https://doi.org/10.1038/s43247-020-0006-x>, 2020

925 ~~57-59.~~ Mariotti, V., Paillard, D., Bopp, L., Roche, D. M., and Bouttes, N.: A coupled model for carbon
 926 and radiocarbon evolution during the last deglaciation. *Geophysical Research Letters*, 43(3), 1306–
 927 1313. <https://doi.org/10.1002/2015GL067489>, 2016.

928 ~~58-60.~~ Marson, J. M., Mysak, L. A., Mata, M. M., and Wainer, I.: Evolution of the deep Atlantic water
 929 masses since the last glacial maximum based on a transient run of NCAR-CCSM3. *Climate Dynamics*,
 930 47(3–4), 865–877. <https://doi.org/10.1007/s00382-015-2876-7>, 2016

931 ~~59-61.~~ Martínez-García, A., Rosell-Melé, A., Jaccard, S.: Southern Ocean dust–climate coupling over
 932 the past four million years. *Nature* 476, 312–315. <https://doi.org/10.1038/nature10310>, 2011.

933 ~~60-62.~~ Martrat, B., Grimalt, J. O., Shackleton, N. J., de Abreu, L., Hutterli, M.A., and Stocker, T. F.: Four
 934 climate cycles of recurring deep and surface water destabilizations on the Iberian Margin, *Science*,
 935 317, 502–507, doi:10.1126/science.1139994, 2007.

936 ~~61-63.~~ Marzocchi, A. and Jansen, M. F. Global cooling linked to increased glacial carbon storage via
 937 changes in Antarctic sea ice. *Nature Geoscience*, 12, 1001–1005, [https://doi.org/10.1038/s41561-](https://doi.org/10.1038/s41561-019-0466-8)
 938 019-0466-8, 2019

939 ~~62-64.~~ Masoum, A., Nerger, L., Willeit, M., Ganopolski, A., and Lohmann, G.: Lessons From Transient
 940 Simulations of the Last Deglaciation With CLIMBER-X: GLAC1D Versus PaleoMist, *Geophysical*
 941 *Research Letters*, 51(16), e2023GL107310. <https://doi.org/10.1029/2023GL107310>, 2024.

942 ~~63-65.~~ McManus, J. F., Francois, R., Gherardi, J.-M., Keigwin, L. D., and Brown-Leger, S.: Collapse
 943 and rapid resumption of Atlantic meridional circulation linked to deglacial climate changes, *Nature*,
 944 428, 834–837, 10.1038/nature02494, 2004.

945 ~~64-66.~~ Menviel, L., Yu, J., Joos, F., Mouchet, A., Meissner, K. J., and England, M. H.: Poorly ventilated
 946 deep ocean at the Last Glacial Maximum inferred from carbon isotopes: A data-model comparison
 947 study. *Paleoceanography*, 32(1), 2–17. <https://doi.org/10.1002/2016PA003024>, 2017.

948 ~~65-67.~~ Menviel, L., Timmermann, a., Timm, O. E., and Mouchet, A.: Climate and biogeochemical
 949 response to a rapid melting of the West Antarctic Ice sheet during interglacials and implications for
 950 future climate. *Paleoceanography*, 25, 1–12. <https://doi.org/10.1029/2009PA001892>, 2010.

951 ~~66-68.~~ Menviel, L., Timmermann, A., Timm, O. E., and Mouchet, A.: Deconstructing the Last Glacial
 952 termination: the role of millennial and orbital-scale forcings, *Quaternary Sci. Rev.*, 30, 1155–1172,
 953 10.1016/j.quascirev.2011.02.005, 2011.

954 ~~67-69.~~ Menviel, L., England, M. H., Meissner, K. J., Mouchet, A., and Yu, J.: Atlantic-Pacific seesaw
955 and its role in outgassing CO₂ during Heinrich events. *Paleoceanography*, 29(January), 58–70.
956 <https://doi.org/10.1002/2013PA002542>, 2014.

957 ~~68-70.~~ Menviel, L., Spence, P., Yu, J., Chamberlain, M. A., Matear, R. J., Meissner, K. J., and England,
958 M. H.: Southern Hemisphere westerlies as a driver of the early deglacial atmospheric CO₂ rise.
959 *Nature Communications*, 9(1), 1–12. <https://doi.org/10.1038/s41467-018-04876-4>, 2018

960 ~~71.~~ Moros, M., De Deckker, P., Perner, K., Ninnemann, U. S., Wacker, L., Telford, R., Jansen, E., Blanz,
961 T. and Schneider, R.: Hydrographic shifts south of Australia over the last deglaciation and possible
962 interhemispheric linkages. *Quaternary Research (United States)*, 102, 130–141.
963 <https://doi.org/10.1017/qua.2021.12>, 2021.

964 ~~72.~~ Morrison, A. and Hogg, A.: On the Relationship between Southern Ocean Overturning and ACC
965 Transport, *J. Phys. Oceanogr.*, 43, 140–148, 2013.

966 ~~69-~~

967 ~~70-73.~~ Moy, A. D., Palmer, M. R., Howard, W. R., Bijma, J., Cooper, M. J., Calvo, E., Pelejero, C.,
968 Gagan, M. K. and Chalk, T. B.: Varied contribution of the Southern Ocean to deglacial atmospheric
969 CO₂ rise. *Nature Geoscience*, 12(12), 1006–1011. <https://doi.org/10.1038/s41561-019-0473-9>, 2019

970 ~~74-74.~~ Ng, H. C., Robinson, L. F., McManus, J. F., Mohamed, K. J., Jacobel, A. W., Ivanovic, R. F.,
971 Gregoire, L. J. and Chen, T.: Coherent deglacial changes in western Atlantic Ocean circulation.
972 *Nature Communications*, 9(1), 1–10. <https://doi.org/10.1038/s41467-018-05312-3>, 2018

973 ~~72-75.~~ Obase, T., and Abe- Ouchi, A.: Abrupt Bølling-Allerød warming simulated under gradual forcing
974 of the last deglaciation, *Geophysical Research Letters*, 46, <https://doi.org/10.1029/2019GL084675>,
975 2019.

976 ~~73-76.~~ Obase, T., A. Abe-Ouchi, F. Saito: Abrupt climate changes in the last two deglaciations simulated
977 with different Northern ice sheet discharge and insolation, *Scientific Reports*, 11, doi:
978 10.1038/s41598-021-01651-2, 2021

979 ~~74-77.~~ Parrenin, F., Masson-Delmotte, V., Köhler, P., Raynaud, D., Paillard, D., Schwander, J., Barbante,
980 C., Landais, A., Wegner, A., Jouzel, J.: Atmospheric carbon dioxide, methane, deuterium, and

書式を変更: フォント: (日) Times New Roman

981 calculated Antarctic temperature of EPICA Dome C ice core. PANGAEA,
 982 doi:10.1594/PANGAEA.810199, 2013

983 ~~75-78.~~ Pedro, J. B., Martin, T., Steig, E. J., Jochum, M., Park, W., & Rasmussen, S. O.: Southern Ocean
 984 deep convection as a driver of Antarctic warming events. *Geophysical Research Letters*, 43(5), 2192–
 985 2199. <https://doi.org/10.1002/2016GL067861>, 2016

986 ~~76-79.~~ Pedro, J. B., Jochum, M., Buizert, C., He, F., Barker, S., & Rasmussen, S. O.: Beyond the bipolar
 987 seesaw: Toward a process understanding of interhemispheric coupling. *Quaternary Science Reviews*,
 988 192, 27–46. <https://doi.org/10.1016/j.quascirev.2018.05.005>, 2018

989 ~~77-80.~~ Peltier, W. R., Argus, D. F., and Drummond, R.: Space geodesy constrains ice age terminal
 990 deglaciation: The global ICE-6G_C (VM5a) model, *J. Geophys. Res.-Sol. Ea.*, 120, 450–487,
 991 10.1002/2014JB011176, 2015.

992 ~~78-81.~~ Petit, J. R., Jouzel, J., Raynaud, D., Barkov, N. I., Barnola, J.-M., Basile, I., Bender, M.,
 993 Chappellaz, J., Davis, M., Delaygue, G., Delmotte, M., Kotlyakov, V. M., Legrand, M., Lipenkov,
 994 V. Y., Lorius, C., Pépin, L., Ritz, C., Saltzman, E., and Stievenard, M.: Climate and atmospheric
 995 history of the past 420 000 years from the Vostok ice core, Antarctica, *Nature*, 399, 429–436,
 996 10.1038/20859, 1999.

997 ~~79-82.~~ Pöppelmeier, F., Jeltsch-Thömmes, A., Lippold, J. et al. Multi-proxy constraints on Atlantic
 998 circulation dynamics since the last ice age. *Nat. Geosci.* 16, 349–356 (2023).
 999 <https://doi.org/10.1038/s41561-023-01140-3>

1000 ~~80-83.~~ Prange, M., Jonkers, L., Merkel, U., Schulz, M. and Bakker, P: A multicentennial mode of North
 1001 Atlantic climate variability throughout the Last Glacial Maximum, *Science*, 9, 44,
 1002 <https://www.science.org/doi/10.1126/sciadv.adh1106>, 2023.

1003 ~~81-84.~~ Rae, J. W. B., Burke, A., Robinson, L. F., Adkins, J. F., Chen, T., Cole, C., Greenop, R., Li, T.,
 1004 Little, E. F. M., Nita, D. C., Stewart, J. A. and Taylor, B. J.: CO₂ storage and release in the deep
 1005 Southern Ocean on millennial to centennial timescales, *Nature*, 562, 569–573,
 1006 <https://doi.org/10.1038/s41586-018-0614-0>, 2018

82-85. Renssen, H., Mairesse, A., Goosse, H., Mathiot, P., Heiri, O., Roche, D. M., Nisancioglu, K. H.
 and Valdes, P. J.: Multiple causes of the Younger Dryas cold period. *Nature Geoscience*, 8(12), 946–
 949. <https://doi.org/10.1038/ngeo2557>, 2015

83-86. Roberts, N. L., Piotrowski, A. M., McManus, J. F., and Keigwin, L. D.: Synchronous Deglacial
 Overturning and Water Mass Source Changes, *Science*, 327, 75–78, 10.1126/science.1178068, 2010.

84-87. Roche, D. M., Renssen, H., Paillard, D., & Levvasseur, G.: Deciphering the spatio-temporal
 complexity of climate change of the last deglaciation: A model analysis. *Climate of the Past*, 7(2),
 591–602. <https://doi.org/10.5194/cp-7-591-2011>, 2011

85-88. Roche, D.M., Wiersma, A.P. & Renssen, H. A systematic study of the impact of freshwater pulses
 with respect to different geographical locations. *Clim Dyn* 34, 997–1013.
<https://doi.org/10.1007/s00382-009-0578-8>, 2010.

86-89. Rojas, M., Moreno, P., Kageyama, M., Crucifix, M., Hewitt, C., Abe-Ouchi, A., Ohgaito, R.,
 Brady E. C. and Hope, P.: The Southern Westerlies during the last glacial maximum in PMIP2
 simulations. *Climate Dynamics*, 32(4), 525–548. <https://doi.org/10.1007/s00382-008-0421-7>, 2009

87-90. Sadatzki, H., Opdyke, B., Menviel, L., Leventer, A., Hope, J. M., Brocks, J. J., Fallon, S., Post,
 A. L., O'brien, P. E., Grant, K., & Armand, L.: Early sea ice decline off East Antarctica at the last
 glacial-interglacial climate transition, *Science Advances*, 9, 41, doi: 10.1126/sciadv.adh9513, 2023.

88-91. Schloesser, F., Friedrich, T., Timmermann, A., DeConto, R. M., and Pollard, D.: Antarctic iceberg
 impacts on future Southern Hemisphere climate, *Nat. Clim. Change*, 9, 672–677,
<https://doi.org/10.1038/s41558-019-0546-1>, 2019.

89-92. Seroussi, H., Nowicki, S., Payne, A. J., Goelzer, H., Lipscomb, W. H., Abe-Ouchi, A., Agosta, C.,
 Albrecht, T., Asay-Davis, X., Barthel, A., Calov, R., Cullather, R., Dumas, C., Galton-Fenzi, B. K.,
 Gladstone, R., Golledge, N. R., Gregory, J. M., Greve, R., Hattermann, T., Hoffman, M. J., Humbert,
 A., Huybrechts, P., Jourdain, N. C., Kleiner, T., Larour, E., Leguy, G. R., Lowry, D. P., Little, C. M.,
 Morlighem, M., Pattyn, F., Pelle, T., Price, S. F., Quiquet, A., Reese, R., Schlegel, N.-J., Shepherd,
 A., Simon, E., Smith, R. S., Straneo, F., Sun, S., Trusel, L. D., Van Breedam, J., van de Wal, R. S.
 W., Winkelmann, R., Zhao, C., Zhang, T., and Zwinger, T.: ISMIP6 Antarctica: a multi-model

ensemble of the Antarctic ice sheet evolution over the 21st century, *The Cryosphere*, 14, 3033–3070, <https://doi.org/10.5194/tc-14-3033-2020>, 2020.

~~90-93.~~ Severinghaus, J. P. and Brook, E. J.: Abrupt Climate Change at the End of the Last Glacial Period Inferred from Trapped Air in Polar Ice, *Science*, 286, 930–934, 10.1126/science.286.5441.930, 1999.

~~91-94.~~ Shakun, J. D., Clark, P. U., He, F., Marcott, S. A., Mix, A. C., Liu, Z., Otto-Bliesner, B., Schmittner, A., and Bard, E.: Global warming preceded by increasing carbon dioxide concentrations during the last deglaciation, *Nature*, 484, 49–54, 10.1038/nature10915, 2012.

~~92-95.~~ Sherriff-Tadano, S., Abe-Ouchi, A., Yoshimori, M., Ohgaito, R., Vadsaria, T., Chan, W-L., Hotta, H., Kikuchi, M., Kodama, T., Oka, A., Southern Ocean surface temperatures and cloud biases in climate models connected to the representation of glacial deep ocean circulation, *Journal of Climate*. 3849-3866, <https://doi.org/10.1175/JCLI-D-22-0221.1>, 2023

~~93-96.~~ Sigman, D. M., Hain, M. P., & Haug, G. H.: The polar ocean and glacial cycles in atmospheric CO2 concentration. *Nature*, 466(7302), 47–55. <https://doi.org/10.1038/nature09149>, 2010

~~94-97.~~ Sikes, E. L., Schiraldi, B., & Williams, A.: Seasonal and Latitudinal Response of New Zealand Sea Surface Temperature to Warming Climate Since the Last Glaciation: Comparing Alkenones to Mg/Ca Foraminiferal Reconstructions. *Paleoceanography and Paleoclimatology*, 34(11), 1816–1832. <https://doi.org/10.1029/2019PA003649>, 2019.

~~95-98.~~ Sime, L. C., Kohfeld, K. E., Le, C., Wolff, E. W., Boer, A. M. De, Graham, R. M., & Bopp, L.: Southern Hemisphere westerly wind changes during the Last Glacial Maximum: model-data comparison. *Quaternary Science Reviews*, 64, 104–120. <https://doi.org/10.1016/j.quascirev.2012.12.008>, 2013.

~~96-99.~~ Skinner, L. C., Fallon, S., Waelbroeck, C., Michel, E., & Barker, S.: Ventilation of the deep Southern Ocean and deglacial CO2 rise. *Science*, 328(5982), 1147–1151. <https://doi.org/10.1126/science.1183627>, 2010

~~97-100.~~ Snoll, B., Ivanovic, R.F., Valdes, P.J., Maycock, A. C. and Gregoire, L. J.: Effect of orographic gravity wave drag on Northern Hemisphere climate in transient simulations of the last deglaciation. *Clim Dyn* 59, 2067–2079. <https://doi.org/10.1007/s00382-022-06196-2>, 2022.

1061 ~~98-101.~~ Snoll, B., Ivanovic, R., Gregoire, L., Sherriff-Tadano, S., Menviel, L., Obase, T., Abe-
1062 Ouchi, A., Bouttes, N., He, C., He, F., Kapsch, M., Mikolajewicz, U., Muglia, J., and Valdes, P.: A
1063 multi-model assessment of the early last deglaciation (PMIP4 LDv1): a meltwater perspective, *Clim.*
1064 *Past*, 20, 789–815, <https://doi.org/10.5194/cp-20-789-2024>, 2024.

1065 ~~99-102.~~ Steffensen, J. P., Andersen, K. K., Bigler, M., Clausen, H. B., Dahl-Jensen, D., Fischer,
1066 H., Goto-Azuma, K., Hansson, M., Johnsen, S. J., Jouzel, J., Masson-Delmotte, V., Popp, T.,
1067 Rasmussen, S. O., Röthlisberger, R., Ruth, U., Stauffer, B., Siggaard-Andersen, M.-L.,
1068 Sveinbjörnsdóttir, Á. E., Svensson, A., and White, J. W. C.: High-Resolution Greenland Ice Core
1069 Data Show Abrupt Climate Change Happens in Few Years, *Science*, 321, 680–684,
1070 10.1126/science.1157707, 2008.

1071 ~~100-103.~~ Stein, K., Timmermann, A., Young Kwon, E., and Friedrich, T.: Timing and magnitude of
1072 Southern Ocean sea ice/carbon cycle feedbacks, *P. Natl. Acad. Sci. USA*, 117, 9,
1073 <https://doi.org/10.1073/pnas.1908670117>, 2020.

1074 ~~101-104.~~ Stocker, T. F., & Johnsen, S. J.: A minimum thermodynamic model for the bipolar seesaw.
1075 *Paleoceanography*, 18(4), 1–9. <https://doi.org/10.1029/2003PA000920>, 2003

1076 ~~102-105.~~ Stouffer, R. J., Yin, J., Gregory, J. M., Dixon, K. W., & Spelman, M. J.: Investigating the
1077 Causes of the Response of the Thermohaline Circulation to Past and. *Journal of Climate*, 19, 1365–
1078 1387. <https://doi.org/10.1002/9781119115397.ch25>, 2006

1079 ~~103-106.~~ Tarasov, L., Dyke, A. S., Neal, R. M., and Peltier, W. R.: A data-calibrated distribution of
1080 deglacial chronologies for the North American ice complex from glaciological modeling, *Earth*
1081 *Planet. Sci. Lett.*, 315–316, 30–40, 10.1016/j.epsl.2011.09.010, 2012

1082 ~~104-107.~~ Tierney, J. E., Zhu, J., King, J., Malevich, S. B., Hakim, G. J., & Poulsen, C. J.: Glacial
1083 cooling and climate sensitivity revisited. *Nature*, 584(7822), 569–573.
1084 <https://doi.org/10.1038/s41586-020-2617-x>, 2020

1085 ~~105-108.~~ Timmermann, A., Timm, O., Stott, L., and Menviel, L.: The roles of CO₂ and orbital
1086 forcing in driving Southern Hemispheric temperature variations during the last 21 000 Yr. *Journal of*
1087 *Climate*, 22(7), 1626–1640. <https://doi.org/10.1175/2008JCLI2161.1>, 2009

1088 ~~106~~109.____ Toucanne, S., Zaragosi, S., Bourillet, J.-F., Marieu, V., Cremer, M., Kageyama, M., Van
1089 Vliet-Lanoë, B., Eynaud, F., Turon, J.-L., and Gibbard, P.-L.: The first estimation of Fleuve Manche
1090 palaeoriver discharge during the last deglaciation: Evidence for Fennoscandian ice sheet meltwater
1091 flow in the English Channel ca 20–18 ka ago, *Earth Planet. Sc. Lett.*, 290, 459–473, 2010.

1092 ~~107~~110.____ WAIS Divide Project Members: Onset of deglacial warming in West Antarctica driven by
1093 local orbital forcing. *Nature*, 500(7463), 440–444. <https://doi.org/10.1038/nature12376>, 2013.

1094 ~~108~~111.____ WAIS Divide project members: Precise interpolar phasing of abrupt climate change during
1095 the last ice age. *Nature*, 520(7549), 661–665. <https://doi.org/10.1038/nature14401>, 2015

1096 ~~109~~112.____ Weitzel, N., Andres, H., Baudouin, J.-P., Kapsch, M.-L., Mikolajewicz, U., Jonkers, L.,
1097 Bothe, O., Ziegler, E., Kleinen, T., Paul, A., and Rehfeld, K.: Towards spatio-temporal comparison
1098 of simulated and reconstructed sea surface temperatures for the last deglaciation, *Clim. Past*, 20, 865–
1099 890, <https://doi.org/10.5194/cp-20-865-2024>, 2024.

1100 ~~110~~113.____ Yoshimori, M., Yokohata, T., and Abe-Ouchi, A.: A Comparison of Climate Feedback
1101 Strength between CO2 Doubling and LGM Experiments, *J. Climate*, 22, 3374–3395,
1102 <https://doi.org/10.1175/2009JCLI2801.1>, 2009.

1103 ~~111~~114.____ Zhu, J. and Poulsen, C. J.: Last Glacial Maximum (LGM) climate forcing and ocean
1104 dynamical feedback and their implications for estimating climate sensitivity, *Clim. Past*, 17, 253–
1105 267, <https://doi.org/10.5194/cp-17-253-2021>, 2021.

1106

1107